robotics

MDPI

Article

Quantum-Inspired Sliding-Mode Control to Enhance the Precision and Energy Efficiency of an Articulated Industrial Robotic Arm

Mehdi Fazilat and Nadjet Zioui *

Université du Québec à Trois-Rivières, Department of Mechanical Engineering, 3351 Bd des Forges, Trois-Rivières, QC G8Z 4M3, Canada; mehdi.fazilat@uqtr.ca
* Correspondence: nadjet.zioui@uqtr.ca

Abstract: Maintaining precise and robust control in robotic systems, particularly those with nonlinear dynamics and external disturbances, is a significant challenge in robotics. Sliding-mode control (SMC) is a widely used technique to tackle these issues; however, it is plagued by chattering and computational complexity, which limit its effectiveness in high-precision environments. This study aims to develop and assess a quantum-inspired sliding-mode control (QSMC) strategy to enhance the SMC's robustness, precision, and computational efficiency, specifically in controlling a six-jointed articulated robotic arm. The methodology involves creating a comprehensive kinematic and dynamic model of the robot, followed by implementing both classic SMC and the proposed Q-SMC in a comparative way. The simulation results confirm that the Q-SMC method outperforms the classic SMC, particularly in reducing chattering, improving tracking accuracy, and decreasing energy consumption by approximately 3.79%. These findings suggest that the Q-SMC technique provides a promising alternative to classical control methods, with potential applications in tasks requiring high precision and efficient robotic manipulations.

Keywords: industrial robotic manipulator arm; kinematics modeling; nonlinear dynamics; sliding-mode control; quantum-inspired sliding-mode control; energy efficiency

Academic Editor: Dan Zhang

Received: 30 December 2024
Revised: 16 January 2025
Accepted: 27 January 2025
Published: 29 January 2025

Citation: Fazilat, M.; Zioui, N. Quantum-Inspired Sliding-Mode Control to Enhance the Precision and Energy Efficiency of an Articulated Industrial Robotic Arm. *Robotics* **2025**, *14*, 14. https://doi.org/10.3390/robotics14020014

1. Introduction

1.1. Context of the Study

Robust control is a key component in robotics, particularly in controlling the complexities of nonlinear dynamics and external disturbances that arise when operating articulated robotic arms. Sliding-mode control (SMC) is well known for its robustness and precision, particularly in managing the nonlinear dynamics and external disturbances encountered when controlling robotic arms. Its ability to maintain stability and performance despite the system's uncertainties makes it particularly ideal for articulated robotic arms with large degrees of freedom [1–4]. SMC accomplishes this by shifting the system's state to a predefined sliding surface, where it can effectively handle variations in the robot's dynamics and external forces applied to tasks such as trajectory tracking, path planning, and force control, ensuring that the robotic arm can execute precise and reliable movements even under challenging conditions [5–7]. However, traditional SMC techniques have substantial limitations, such as chattering and computing complexity, which limit

their practical implementation in high-precision and dynamic situations [8–10]. To address these challenges, the current study provides a robust sliding-mode controller with chattering rejection capabilities and suggests a quantum-inspired sliding-mode control approach designed for a six-degree-of-freedom articulated robotic arm. The work advances the field by constructing a thorough kinematic and dynamic model of the robot using precise CAD designs from SolidWorks software 2024 SP4.0 to extract mass properties required for correct path planning and trajectory execution and evaluating the practice's performance parameters [11]. A unique quantum control algorithm employing multiple qubit operators is also developed, which improves the robustness of the control strategy. This novel approach improves the robustness and precision of the control system, considerably boosting the robot's energy efficiency performance, as evidenced by rigorous testing. Integrating the quantum principles into SMC is a novel advancement in robotic arm control, opening new avenues for overcoming the constraints of traditional approaches to create more efficient and adaptive robotic systems.

1.2. Related Works

The integration of backstepping terminal sliding-mode control with radial basis function neural networks, as demonstrated by Vijay and Jena [12], highlights the application of SMC in controlling specific objects of a robot manipulator with three degrees of freedom (DOF) in an overhead transmission; however, challenges such as parameter tuning and computational complexity have not been solved. Similarly, Adhikary and Mahanta [13] introduced an adaptive backstepping SMC with time delay estimation, enhancing trajectory tracking and disturbance rejection in two-DOF robotic manipulators, though real-time implementation poses challenges. Norsahperi and Danapalasingam [14] advanced the field by proposing an improved optimal integral SMC to reduce the tracking error and energy consumption in robotic manipulators. This has been validated through simulations on a two-DOF manipulator, with significant potential for industrial applications. Nguyen et al. [15] developed a backstepping global fast terminal sliding-mode control, addressing chattering and enhancing transient response in a two-DOF robotic manipulator, although uncertainty estimation remains challenging. Baek et al. [16] contributed with their widely and stable adaptive SMC, focusing on a two-link planar robot manipulator, demonstrating adaptability with challenges in tuning and convergence. Further advancing SMC, Baek and Kwon [17] introduced a strong and stable adaptive SMC, enhancing disturbance rejection and minimizing chattering in robotic manipulators, particularly in dynamic uncertainty environments. Feng et al. [18] addressed chattering mitigation through full-order SMC with time-varying gains applied to a two-DOF robotic manipulator. At the same time, Zhai and Li [19] focused on high-speed and high-precision applications through fast-exponential SMC, integrating a super-twisting controller with a high-order sliding-mode observer. Soriano et al. [20] shifted the focus to energy efficiency, proposing an optimized SMC using a bat algorithm to reduce energy consumption in a SCARA robot, emphasizing the importance of sustainability in industrial robotics. The integration of neural networks with SMC has also seen considerable advancements, with Yen et al. [21] combining recurrent fuzzy wavelet neural networks with adaptive SMC to enhance tracking accuracy and stability in industrial robots. At the same time, Jung [22] used radial basis function-like neural networks in neuro-sliding-mode control for a three-link rotary robot manipulator, refining SMC gain selection. Gambhire et al. [23] provided a broader perspective by examining the evolution of SMC techniques, including integrating intelligent control strategies such as neural networks, emphasizing the need for robust control mechanisms. Yu et al. [24] extended the discussion with a comprehensive overview of terminal SMC, suggesting an integration with artificial intelligence techniques to enhance adaptability and robustness. Finally, Yin et al. [25] introduced a compensation

SMC with a nonlinear disturbance observer for machining robotic manipulators, significantly improving tracking accuracy and robustness, particularly in industrial applications. The literature on SMC techniques in robotics indicates a clear trend toward more adaptive, intelligent, and energy-efficient control methods, with ongoing research focusing on optimizing real-time implementation and integrating advanced computational techniques to address persistent challenges such as chattering, uncertainty estimation, and energy consumption.

Quantum-inspired SMC denotes a substantial upgrade in control techniques. It aims to manage the limitations of the classic SMC, such as chattering, robustness against disturbances, and computational efficiency. Incorporating quantum principles into SMC offers new possibilities for enhancing the precision and robustness of science and engineering, especially in robotic systems, making it a promising area for prospective investigation.

Early applications of quantum methods in robotics demonstrate the potential of quantum SMC to make fundamental transformations in control systems. For example, Gan et al. [26] integrated quantum-behaved particle swarm optimization with SMC to improve control systems for unmanned underwater vehicles, focusing on enhancing robustness in complex underwater environments. Similarly, Fazilat et al. [27] developed a quantum-based kinematic model for industrial robotic arms, such as the ABB IRB140, seriously reducing computational demands and facilitating real-time processing. Zioui et al. [28] further contributed by modeling rigid body orientation using quantum spins, a crucial aspect of robotics that simplifies spatial orientation modeling and bridges classical and quantum control systems. The development of quantum algorithms and their application in robotics has shown notable promise. Boudjoghra et al. [29] introduced a quantum computing-based solution using the Harrow–Hassidim–Lloyd (HHL) algorithm to address state-domain equations in control theory. This approach is particularly beneficial for dynamic systems in robotics, reducing computational intricacy. Singh and Sloth [30] developed an evolving type 2 quantum fuzzy neural network for robotic manipulators, integrating quantum fuzzy logic with traditional neural networks to enhance adaptability and stability. State-of-the-art applications of quantum control in robotics are beginning to emerge, showcasing the potential of these methods to enhance performance in problematic environments. Zheng and Su [31] used QPSO to enhance SMC for electro-hydraulic servo systems, achieving significant improvements in tracking accuracy and setting a benchmark for optimizing control in uncertain robotic environments. Qu et al. [32] introduced a novel integral SMC for helicopter systems, integrating quantum information techniques to improve control accuracy and disturbance rejection, which is crucial for dynamic robotic systems like helicopters. In another investigation, Zioui et al. [33] extended quantum computing applications in robotic kinematics by developing a quaternion model for robotic arm positioning, demonstrating the feasibility of quantum models in practical robotics and paving the way for future Q-SMC strategies. The impact of quantum-inspired control methods on robotics is increasingly evident as researchers explore their adaptability and efficiency. Sivak et al. [34] proposed a model-free quantum control approach using reinforcement learning, enhancing the adaptability and performance of quantum-based control methods in environments where precise models are challenging to obtain. Quantum computing's potential to revolutionize robotics is further highlighted by Petschnigg et al. [35], who synthesized the current state of quantum computing and proposed its application to complex robotic challenges like AI, machine learning, and kinematics. Niu et al. [36] involved quantum control through deep reinforcement learning to optimize quantum systems, offering insights into adapting these methods for robotic applications that require real-time decision-making under uncertainty. Specialized quantum control strategies for robotics continue to advance the field. Reshetnikov and Ulyanov [37] explored

the application of quantum fuzzy controllers in robotic systems like mobile manipulators, demonstrating marked control accuracy and robustness improvements. Tavanaei-Sereshki and Ramezani-al [38] developed a quantum genetic algorithm-based SMC for autonomous underwater vehicles, showing superior performance in nonlinear, dynamic surroundings and highlighting the broader applicability of quantum-inspired control strategies in other robotic systems. The study by Xi et al. [39] addresses the significant challenge of controlling robot manipulators in industrial environments characterized by high uncertainties and nonlinear dynamics. Their robust adaptive SMC system integrates an adaptive sliding-mode disturbance observer with backstepping techniques, demonstrating enhanced precision and stability in uncertain environments. The reviewed studies collectively illustrate the transformative potential of quantum SMC in various aspects of intelligent mechanisms and robotics. By addressing challenges in traditional control methods, from high-dimensional optimization to real-time adaptation in dynamic environments, these studies contribute to a growing body of knowledge that could significantly influence overcoming the limitations of classical methods, enhancing the precision, robustness, and computational efficiency of robotic control systems.

1.3. Problem Formulation and Contribution

While SMC has proven to be a robust solution for managing the nonlinear dynamics and external disturbances in robotic arms, significant limitations such as chattering and computational complexity persist. These issues hinder the practical application of SMC in high-precision, dynamic environments, particularly in robotics systems with high degrees of freedom. More adaptive, precise, and computationally efficient control strategies still need to be met, especially in scenarios requiring real-time response and energy efficiency. It is essential to investigate filling this gap by exploring the potential of quantum-inspired sliding-mode control to examine the probability of overcoming these intrinsic limitations.

The primary purpose of the current examination is to develop and validate a novel quantum-enhanced sliding-mode control strategy, particularly for a six-degree-of-freedom articulated robotic arm and perform a comparative study between the performance of classic SMC and a quantum version of sliding-mode control. It aims to enhance SMC's robustness, precision, and computational efficiency by integrating quantum principles into the control strategy, focusing on addressing the persistent issues of chattering, computational complexity, and robustness against disturbances, which are vital for achieving high-performance robotic control to improve the control system's energy efficiency and adaptability, ultimately contributing to more reliable and efficient robotic arm manipulations in dynamic environments.

The effectiveness of this study lies in its possibility of enhancing control systems in robotics by introducing quantum-inspired sliding-mode control as a practicable alternative to classic methods. Incorporating quantum principles into SMC could increase robotic systems' performance and energy efficiency by addressing the evolution of computational methodologies. It offers a more robust and precise control strategy that can be applied in applications, particularly in the adaptability and effectiveness of robotic systems in real-world scenarios where precision, speed, and reliability are paramount.

The present study compares two control strategies, the classical sliding-mode control and its quantum-inspired sliding-mode control counterpart. The primary objective was to evaluate the integration of quantum principles into control methodologies and assess its potential to enhance performance. In this comprehensive case study, we developed a robust SMC-based control framework for our robotic arm and extended it to include quantum-inspired elements. While acknowledging the effectiveness of other advanced control strategies such as Model Predictive Control, reinforcement learning-based methods, Adaptive Control, Fractional Order Control, and H-infinity Robust Control, we notice the

significance of exploring these approaches to broaden the comparative scope of our research. However, for this study, we focused on a singular, well-established control strategy and its quantum-inspired enhancement to facilitate a concentrated and stringent analysis of their respective performance.

The current research presents a comprehensive study of robust control of an industrial manipulator robotic arm incorporating quantum-inspired sliding-mode control for robotic arms. Section 2 explores the kinematic modeling of the ABB IRB140 robot, emphasizing an advanced approach to developing a precise model for motion planning and performance evaluation. This section also details the CAD design of the robotic arm, underscoring the critical importance of accurately obtaining mass properties. Furthermore, it outlines the design of a robust SMC strategy, including techniques for reducing chattering and introducing a novel quantum-inspired sliding-mode control algorithm employing multiple qubit operators. Section 3 presents the experimental results, demonstrating the superior performance of the quantum-enhanced SMC in managing the manipulator robot arm. Finally, Section 4 discusses the implications of these findings and suggests directions for future research in the control of robotics and quantum computing.

2. Methodology

2.1. Robotic Arm Presentation

The study focuses on the ABB IRB 140 robot, illustrated in Figure 1. This si*x*-axis articulated robot is widely employed in different industrial applications. According to ABB's technical specifications, it provides flexible mounting options, such as floor, wall, and inverted positions, to accommodate different working environments. The IRB 140 robot is commonly utilized for arc welding, assembly, material handling, machine tending, cleaning, and spraying, packing, and deburring. With a weight of approximately 98 kg, it can support an end-effector with a payload capacity of up to 5 kg. The robot's reach extends to about 810 mm at its mounting flange, and it can bear up to 1.5 kg of equipment on its upper arm. The joint limits offer a significant functional workspace, as outlined in Table 1 [11].

Figure 1. The ABB IRB 140 robot located in the UQTR automation laboratory.

Table 1. Joint limits of the ABB IRB 140 robot.

Joints	Type of the Joint	Limits (°)
1	R	+180 to −180
2	R	+110 to −90

3	R	+50 to −230
4	R	+200 to −200
5	R	+120 to −120
6	R [1]	+400 to −400

[1] R stands for rotational or revolute.

The robotic arm features an IRC5 advanced controller designed to handle multiple robots, optimizing their performance for shorter cycle times and precise movements. It also incorporates RobotWare (Robot Studio), allowing ABB robots to be programmed from a workstation without disrupting active production processes. This configuration includes the ABB Virtual Controller, a representation of the production-level software that enables program development. Robot Studio presents highly realistic simulations, utilizing simple robot programs and configuration files that accurately reflect real-world operations [11].

For the present research, the ABB IRB 140 robot was utilized in its original configuration, strictly following the manufacturer's specifications. The robot's structure and system remained unchanged, with no custom modifications. This approach ensures that our study's results and insights accurately reflect the standard performance of the ABB IRB 140 as commonly observed in industrial settings. Additionally, it provides a baseline for evaluating the robot's efficiency and dynamics in typical operational scenarios.

2.2. Mathematical Model of the Robot

The evaluation of the ABB IRB-140 robotic arm at the UQTR mechatronic laboratory began by inputting joint-specific data to generate trajectories, which served as a foundation for implementing kinematic models. These models were developed using Denavit–Hartenberg parameters (Table 2) to define the position and orientation of the end-effector. The robot's joint motions were generated using fifth-order polynomial equations and transformation matrices, allowing for a detailed description of the potential positions and orientations. This kinematic analysis was a prototype of dynamic modeling, which employed the Euler–Lagrange method to explore the robot's dynamics, focusing on joint torque calculations and energy consumption. The dynamic model was further enhanced by incorporating inertia and mass center point data from detailed CAD/CAM designs created using SolidWorks software. This phase seamlessly transitioned into computer-aided optimization (CAO), enabling comprehensive simulations representing various model fidelity levels. Integrating kinematic and dynamic models facilitated a comprehensive analysis, allowing precise estimation of the robot's energy needs through torque profiles.

Table 2. Denavit–Hartenberg Parameters of the ABB IRB 140 [11,28].

Link	a (mm)	α (°)	d (mm)	q (°)
1	a_1 = 70	−90	d_1 = 352	q_1
2	a_2 = −360	0	0	q_2 + 90
3	0	−90	0	q_3
4	0	90	d_4 = 380	q_4
5	0	−90	0	q_5
6	0	0	d_6 = 65	q_6

After that, the inverse kinematics was developed. The model involves determining the joint angles that achieve a specific end-effector position. This model is crucial for maintaining safe and reliable robot operations but also allows for explicit control over the robot's posture. Additionally, it offers a computationally efficient method for determining

joint angles, making them particularly beneficial in real-time control scenarios where rapid computation is essential.

The differential kinematics was also developed to define how the angular velocities of a robot's joints relate to its end-effector's linear and angular velocities. By analyzing velocities and static forces, the Jacobian matrix J of the manipulator is derived. This matrix plays a key role in examining and controlling robotic motion, identifying singularities and redundancy, formulating inverse kinematic equations, and characterizing the manipulability of velocity and force [40]. The Jacobian matrix is specifically adapted to the unique joint configurations of each robot, greatly enhancing motion planning and control, which are essential for executing precision tasks. It also addresses singularities and redundancies, improving the robot's operational efficiency and safety.

Finally, a dynamic model is developed to enable the analysis of a robot's performance regarding joint acceleration forces and torques. The Euler–Lagrange method is commonly employed to establish such a dynamic model. The first three proximal joints are fundamental as they play a significant role in assessing the mechanical loads experienced by the mechanical structure of the robot during operation, which is a key factor in the dynamic modeling and assumptions made in the model. The dynamic behavior of a robotic arm with n joints can be described by relation (1) [11].

$$M\ddot{q} + V + G = \tau \quad (1)$$

In this context, $\ddot{q}$ represents the joint acceleration vector, M is the inertia matrix, V corresponds to the Coriolis vector, G denotes the gravitational vector, and τ is the force and torque vector. In our study, the elements of the inertia matrix and the positions of the mass centers were determined using SolidWorks software. The uniform density assumption for each link was applied across all models. It also considered key values related to mass and other physical properties, such as the mass center positions and inertia matrices, represented within their respective reference frames for the three proximal links. The precision of a dynamic model relies heavily on accurately determining mass centers and inertia matrices. To obtain these necessary data in engineering, straightforward dimensional specifications, and scientific methods, including CAD modeling, Experimental Modal Analysis, and Inertia Measurement Units, are utilized. CAD modeling provides detailed information on dimensions and mass distribution, while Experimental Modal Analysis and Inertia Measurement Units offer direct measurements of inertia characteristics. The mass of each link can be calculated assuming constant and uniform density. SolidWorks software was utilized to determine the volume of each link. The mass of each link is estimated by multiplying the ratio of an individual link's volume to the total robot volume by the total robot mass.

2.3. CAD Designs of the Robot

Employing SolidWorks, we performed a high degree of precision in modeling each robotic arm component. A determined purpose of accuracy and steady state to our conceptual design parameters depicted our methodology. This introductory phase has specified a solid foundation for a robotic arm balanced to enhance the capabilities within industrial automation, mainly characterized by its superior functionality. During the CAD design process, we make the simplifying assumption that the robot's components have a uniform density. While this assumption simplifies the calculations, it may result in inaccuracies since it must account for the material variations in the real robot. Additionally, ergonomics and safety were essential throughout the design iterations, driven by an iterative process. This process concerned rigorous stress examination, evaluation of energy consumption patterns, and comprehensive persistence testing. These steps were required to establish the arm's mechanical robustness and stable reliability, ensuring its

appropriateness for reinforcing industrial application. The precise, detailed model depicted in Figure 2 is fundamental for the simulations that require high fidelity and detailed analysis. This model reproduces the robot's configuration with maximum accuracy, making it ideal for investigating elaborate dynamics and interactions within the real robot's mechanism. Mass and inertia values are established on the presumed material properties and the model's geometry. These values are essential for dynamic simulations, but they may not fully reflect the actual robot due to potential manufacturing variations and inconsistencies in material properties [11].

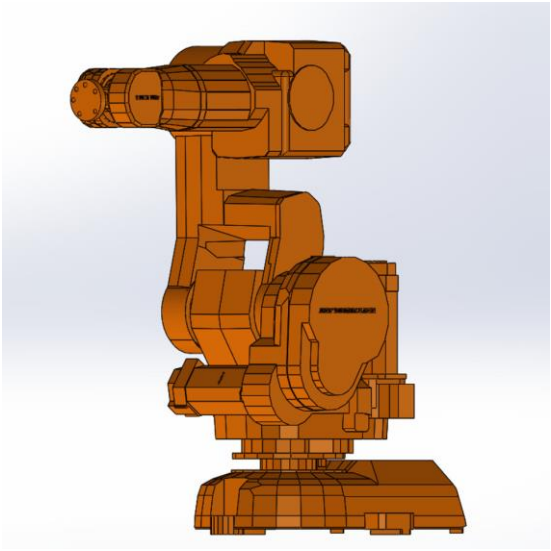

Figure 2. Detailed SolidWorks model of the ABB IRB 140 robotic arm [11].

The specifics of the model and the results for the proximal links obtained using the mass properties tool are outlined in Table 3 [11].

Table 3. Mass property results of each model calculated using SolidWorks software [11].

ABB IRB 140	Parameters (Unit)	Link 1	Link 2	Link 3
Mass Properties	*Weight* (kg)	35	25	18
	Xc (mm)	277.87	218.29	−24.56
	Yc	373.12	229.73	−219.9
	Zc	−199.03	112.43	−25.86
	Ixx (kg·m²)	6.5	0.9	2.5
	Ixy	1.1	−0.03	−0.001
	Ixz	3.05	0.1	0.09
	Iyy	2.02	1.3	2.7
	Iyz	5.07	−0.01	−0.8

2.4. Robot Performance Assessment

To evaluate the accuracy of the three models' predictions, we analyzed the energy consumption by the three proximal joints and the robot's total energy consumption over the same duration and path of movement. In the proposed modeling approach, the energy consumption of each joint at a specific time can be calculated from the joint torque and angular velocity using Equation (2). The robot's integrated energy consumption is assumed to be the sum of the energy consumption values of all the joints.

$$E_i = \int_{t_0}^{t_f} \tau_i(t).\dot{q}_i(t)\, dt \quad (2)$$

We employ a theoretical approach to evaluate the energy consumption of robotic arms. This approach centers on dynamic models that simulate each joint's torque τ_i and angular velocity $\dot{q}_i$ Detailed explanations of how these parameters are simulated are provided in the methodology section. The simulated values are then used in Equation (2) to calculate the energy consumption of each joint. The theoretical method offers a comprehensive analysis of energy consumption, avoiding the practical challenges and complexities associated with the installation and calibration of physical sensors on the robotic arm.

Focusing on a theoretical and simulation-based approach contributes significantly to understanding energy dynamics in robotic arms, especially in scenarios where direct measurement is impractical or impossible. This approach also aligns with current trends in employing computational models to analyze complex system contributions to robotics fields.

2.5. Sliding-Mode Control Strategy

One method of robust control technique for controlling a complicated and nonlinear mechanism like a manipulator robotic arm is called sliding-mode control methodology, a type of variable structure control system [4,10,41]. The most crucial feature of the sliding-mode control is the complete insensitivity to parametric uncertainty and external disturbances during the sliding process. The variable structure control system utilizes a high-speed switching-control law for two purposes. First of all, it forces the nonlinear system's form trajectory along a user-defined surface in the state space, named the sliding or switching surface [42,43]. The control approach has one gain if the state trajectory of the mechanism is above the surface and a different gain if the controlling object, such as trajectory in robotics, drops below the surface and because of this named sliding surface. Secondly, it keeps the mechanism state control object on this surface by following the time [44,45]. During the controlling process, the control system's structure differs from one to another and thus it donates the name variable structure control. This model also permits the elimination of interactions among the joints of the manipulator [46,47]. A general equation of the motion can be represented in the space state by the following [48]:

$$x = f(x,t) + g(x,t).u \tag{3}$$

where u is the control input, x is the state vector also considered as the output, and the functions $f(x,t)$ and $g(x,t)$ are nonlinear functions.

The control input variable is defined in the following:

$$u_i(x,t) = \begin{cases} u_i^+(x,t) & if\ \ S_i(x,t) > 0 \\ u_i^-(x,t) & if\ \ S_i(x,t) < 0 \end{cases} \tag{4}$$

where u_i, is the i^{th} component of u, and $S_i(x,t) = 0$ is the i^{th} component-switching hypersurfaces $S(x, t) = 0$, $S \in R^m$.

According to the presented rules with discontinuous control, the system is named a variable structure system since the controller switches alternatively based on the state of the mechanism. The sliding mode appears on a switching surface $S(x) = 0$, which pushes the machine to behave as a linear-time uniform system, which can be assumed to be stable. For it to be linear, the surfaces can be written as:

$$s_i(x) = x_n + \sum_{i=1}^{n} \lambda_i . x_i \tag{5}$$

The condition for the sliding mode to exist on the i^{th} surface is provided by the following equation:

$$\lim_{s_i \to 0^+} \dot{S} > 0 \quad \text{and} \quad \lim_{s_i \to 0^-} \dot{S} < 0 \tag{6}$$

This is when $S\dot{S} < 0$ is too close to $S_i(x) = 0$, when all the trajectories shift towards the switching surface. In the perfect sliding mode on S_i, the related control is the equal control issued from Equation (3) and given by the equation for $\dot{S} = 0$:

$$u_{eq} = g^{-1}(x,t)[\dot{x}(t) - f(x,t)] \tag{7}$$

So, the discontinuous control input presented in relation (4) can be noted as follows:

$$u_i = \begin{cases} u_{ieq}^* + \Delta u_i^+ & if\ \ S_i > 0 \\ u_{ieq}^* + \Delta u_i^- & if\ \ S_i < 0 \end{cases} \tag{8}$$

where u_{eq} illustrates the low-frequency control component or the steady state equivalent control signal, and Δu presents the high-frequency discontinuous term. For the functional case, the control equation is known by the evaluated value due to error modulization and variation in the parameters as follows:

$$u_{eq}^* = u_{eq} + \Delta u_{eq} \tag{9}$$

This last formula is equivalent to the discontinuous control input in relation (8). The term of high-frequency Δu can be represented differently, such as the equation based on the classical reaching law, which is one of the methods reported in the literature for alleviating chattering in sliding mode. Classical reaching law can express in four principal subcategories that are represented as the following:

Constant reaching law:

$$\dot{s} = -\varepsilon.sgn(s)\,, \qquad \varepsilon > 0 \tag{10}$$

Exponential reaching law:

$$\dot{s} = -\varepsilon.sgn(s)\ - ks, \qquad \varepsilon > 0 \qquad k > 0 \tag{11}$$

Power-rate reaching law:

$$\dot{s} = -k\,|s^{\alpha}|.sgn(s), \qquad 0 <\ \alpha < 1 \qquad k > 0 \tag{12}$$

General reaching law:

$$\dot{s} = -\varepsilon.sgn(s) - f(s)\ \ ,\varepsilon > 0\ \ \text{where}\ f\ (0)\ = 0\ \text{and}\ sf(s) > 0\ \text{when s}\ \neq\ 0 \tag{13}$$

To obtain a robust sliding-mode control based on reaching law, consider the general equation motion as below:

$$\ddot{x} = f(x) + g(x)u + d(t) \tag{14}$$

where $f(x)$ and $g(x)$ are unknown equations and $g(x) > 0$ and $d(t)$ are the terms of disturbance. As sliding surface and derivative of the sliding surface, the combination of error of models considered satisfy the Hurwitz condition and can be described as follows:

$$s = \dot{e} + ce, c > 0 \tag{15.1}$$

$$e = r - x(t) \tag{15.2}$$

$$\dot{e} = \dot{r} - \dot{x}(t) \tag{15.3}$$

For the derivative of the sliding-surface equation considering the effect of external disturbance as $d(t)$:

$$\dot{s} = \ddot{e} + c\dot{e} = \ddot{r} - \ddot{x} + c(\dot{r} - \dot{x}) = \ddot{r} - f(x) - g(x)u - d(t) +\ c(\dot{r} - \dot{x}) \tag{16}$$

To obtain the robust control sliding mode based on the exponential reaching law from the relations of (12) and (16):

$$\ddot{r} - f(x) - g(x)u - d(t) + c(\dot{r} - \dot{x}) = -\varepsilon.sgn(s) - ks$$
$$u = \frac{1}{g(x)}(\ddot{r} - f(x) - d(t) + c(\dot{r} - \dot{x}) + \varepsilon.sgn(s) + ks \quad (17)$$

The derivative of the sliding-surface equation can also be considered with (15) described with the disturbance term as follows:

$$\dot{s} = -\varepsilon.sgn(s) - ks + d_c - d \quad (18)$$

The disturbance term d_c must satisfy the conditions for reaching the sliding surface, and the term d should be limited. dl and du are the lower and upper terms of disturbance, respectively, as:

$d_l \le d(t) \le d_u$, when s(t) > 0, $\dot{s} = \varepsilon - ks + d_c - d$, we want $\dot{s}$(t) < 0, so let $d_c = d_l$.

When s(t) < 0, $\dot{s} = -\varepsilon - ks + d_c - d$, we want $\dot{s}$(t) > 0, so let $d_c = d_u$

Therefore, if we define $d_1 = \frac{d_u - d_l}{2}$, $d_2 = \frac{d_u + d_l}{2}$, then we can obtain the following:

$$d_c = d_2 - d_1.sgn(s) \quad (19)$$

The discontinuity of the sign function will generate chattering in the closed loop system. For this reason, the sign function is usually substituted by a saturation function sat (s/ε), where $sat(.)$ is described as follows:

$$sat(x) = \begin{cases} x & if\ |x| \le 1 \\ sgn\,(x) & if\ |x| > 1 \end{cases} \quad (20)$$

To mitigate chattering, the study employs an exponential reaching law, which adjusts the conventional reaching law to achieve a smoother transition as the system state approaches the sliding surface. This is accomplished by adding a term, $-k \cdot s$, which gradually decreases the convergence rate to the sliding surface, thereby reducing the rapid switching responsible for chattering. Additionally, the discontinuous sign function $sgn\,(s)$ is replaced with a saturation function sat (s/ϵ), which introduces a boundary layer around the sliding surface. This change smooths the control action, significantly curbing chattering by preventing abrupt changes in the control input. By adjusting the thickness of this boundary layer, the system can strike an optimal balance between reducing chattering and maintaining precise control, enhancing the robustness and applicability of SMC in high-precision environments.

Employing this alternate will present a tracking error. The trade-off between the tracking error and control bandwidth will be created by setting the boundary layer properly. As mentioned before, the position of the robot's end-effector in this case study depends on the first three joints and links. For this reason, the control strategy implements the first three joints of the robot. Generally, for the three links, the robot's sliding-mode control can be described as follows:

$$s = \dot{e} + ce \quad (21)$$

For example, $e = \theta_d - \theta$.

This will lead to $\dot{s} = \ddot{e} + c\dot{e} = \ddot{\theta_d} - \ddot{\theta} + c\dot{e}$ and

$$\dot{s} = -\varepsilon\, sgn(s) \quad (22)$$

The combination of Equations (21) and (22) will result in the following:

$$\ddot{\theta} = \ddot{\theta_d} + c\dot{e} + \varepsilon\, sgn\,(s) \quad (23)$$

The general equation of the robot relies on the dynamics of the robot described as relation (1), which can be rewritten in terms of accelerations as the following:

$$\ddot{\theta} = M^{-1}(\tau - V - G) \tag{24}$$

With relations (23) and (24), we obtain the main equation of sliding-mode control as follows:

$$\tau = M\left(\ddot{\theta_d} + c\dot{e} + \varepsilon\, sgn(s)\right) + V + G \tag{25}$$

Assuming the presence of the disturbances for the robot in the working space to determine and track of end-effector position and considering inverse kinematics and dynamics of the robot manipulator, we can achieve the following equation for controlling in the sliding-mode technique:

$$\tau = M.J^{-1}\left(\ddot{X}_d + c\dot{e} + \varepsilon\, sgn(s) - \dot{J}(\theta)\dot{\theta}\right) + V + G \tag{26}$$

2.6. Quantum Computing Basics

Quantum computing operates on a different principle compared to classical computing, utilizing quantum bits, or qubits, to encode and process information. A qubit state, denoted as $|q\rangle$, can be expressed as a superposition of the classical binary states 0 and 1 [49,50]. Mathematically, this is represented as:

$$|q\rangle = \alpha|0\rangle + \beta|1\rangle \tag{27}$$

Here, α and β are complex coefficients that correspond to the probability amplitudes of the qubit being in the states $|0\rangle$ and $|1\rangle$, respectively. These probabilities can be interpreted such that $|\alpha|^2$ gives the likelihood of the qubit being in the $|0\rangle$ state, while $|\beta|^2$ gives the probability of it being in the $|1)$ state. In the context of vector space, the states $|0\rangle$ and $|1\rangle$ can be represented as the vectors $|0\rangle \equiv \binom{1}{0}$ and $|1\rangle \equiv \binom{0}{1}$, respectively [49,50]. Thus, a qubit state $|q\rangle$ can be depicted in vector form as $\binom{\alpha}{\beta}$. Quantum operations, known as quantum gates, can be applied to qubits to alter their states. These operations are often represented by Hamiltonian matrices [28,33]. The fundamental quantum gates that act on a single qubit include the identity, X, Y, and Z gates, which correspond to the Pauli matrices σ_0, σ_x, σ_y, and σ_z, respectively, as defined by the following matrices [50]:

$$\sigma_0 = \begin{pmatrix} 1 & 0 \\ 0 & 1 \end{pmatrix} \tag{28}$$

$$\sigma_x = \begin{pmatrix} 0 & 1 \\ 1 & 0 \end{pmatrix} \tag{29}$$

$$\sigma_y = \begin{pmatrix} 0 & -i \\ i & 0 \end{pmatrix} \tag{30}$$

$$\sigma_z = \begin{pmatrix} 1 & 0 \\ 0 & -1 \end{pmatrix} \tag{31}$$

Other single-qubit quantum gates can be expressed as a linear combination of the Pauli gates, such as the Hadamard gate depicted in Equation (32) and the three basic rotation gates illustrated in Equations (33)–(35) [51,52].

$$H = \frac{\sqrt{2}}{2}\begin{pmatrix} 1 & 1 \\ 1 & 1 \end{pmatrix} = \frac{\sqrt{2}}{2}(\sigma_0 + \sigma_x) \tag{32}$$

$$R_x(\theta) = \begin{pmatrix} cos\theta & -i\, sin\theta \\ -i\, sin\theta & cos\theta \end{pmatrix} = cos\theta\ \sigma_0 - i\, sin\theta\ \sigma_x \tag{33}$$

$$R_y(\theta) = \begin{pmatrix} cos\theta & -sin\theta \\ sin\theta & cos\theta \end{pmatrix} = cos\theta\ \sigma_0 - i\ sin\theta\ \sigma_y \quad (34)$$

$$R_z(\theta) = \begin{pmatrix} e^{-i\theta} & 0 \\ 0 & e^{i\theta} \end{pmatrix} = cos\theta\ \sigma_0 - i\ sin\theta\ \sigma_z \quad (35)$$

2.6.1. Developing the Quantum Comparator

The quantum comparator is an innovative computational tool that harnesses quantum principles to enhance precision and efficiency in comparison tasks. It integrates two primary components: a quantum subtractor and a quantum sign detector [50].

The quantum subtractor computes the difference between two real numbers. Operating within the quantum framework, it offers higher parallelism and potentially faster speeds than classical subtractors. This enables it to prepare the data for the next step by providing the relative magnitude of the two numbers. Once the subtraction is complete, the result is passed to the quantum sign detector. This component determines the sign of the computed difference, indicating whether the first number is more significant than, less than, or equal to the second number. By leveraging quantum superposition and entanglement principles, the quantum sign detector identifies the sign accurately and efficiently, completing the comparison. These components work together to enable the quantum comparator to perform comparisons with greater accuracy and speed than classical methods, making it a valuable tool in quantum computing applications [53–55].

2.6.2. The Quantum Subtractor

The quantum subtractor for two real numbers relies on the tensor product between two real qubit states, $q_1 = C_{\theta_1}|0\rangle + S_{\theta_1}|1\rangle$ and $q_2 = C_{\theta_2}|0\rangle + S_{\theta_2}|1\rangle$. These qubit states, q_1 and q_2, are derived by applying a quantum rotation around the y-axis, as described by the following equations:

$$q_1 = R_y(\theta_1)|0\rangle \quad (36)$$

$$q_2 = R_y(\theta_2)|0\rangle \quad (37)$$

The tensor product between q_1 and q_2 yields the coefficients of the eigenstates:

$$q_1 \otimes q_2 = C_{\theta_1}C_{\theta_2}|00\rangle + C_{\theta_1}S_{\theta_2}|01\rangle + S_{\theta_1}C_{\theta_2}|10\rangle + S_{\theta_1}S_{\theta_2}|11\rangle \quad (38)$$

The coefficient $S_{\theta_1}C_{\theta_2}$ can be obtained by measuring the system $q_1 \otimes q_2$ in the state $|10\rangle$. This coefficient can be rewritten using the trigonometric identity:

$$S_{\theta_1}C_{\theta_2} = \sin\left(\frac{\alpha-\beta}{2}\right)\cos\left(\frac{\alpha+\beta}{2}\right) = \frac{1}{2}(\sin(\alpha) - \sin(\beta)) \quad (39)$$

where $\frac{\alpha-\beta}{2} = \theta_1$ and $\frac{\alpha+\beta}{2} = \theta_2$, with $\alpha = \theta_1 + \theta_2$ and $\beta = \theta_2 - \theta_1$.

Thus, the subtraction of two real numbers $x = \sin(\alpha)$ and $y = \sin(\beta)$ can be computed through the following steps:

Step 1: Compute $\alpha = \arcsin(x)$ and $\beta = \arcsin(y)$.

Convert the input numbers x and y into angles α and β, which will be used for quantum operations.

Step 2: Determine θ_1 as $\frac{\alpha-\beta}{2}$ and θ_2 as $\frac{\alpha+\beta}{2}$.

This calculates the rotation angles θ_1 and θ_2, encoding the difference and sum of the input numbers.

Step 3: Initialize the qubits q_1 and q_2 to $|0\rangle$.

This prepares the qubits in a known starting state before any quantum operations are applied.

Step 4: Apply the quantum rotations $R_y(\theta_1)$ to q_1 and $R_y(\theta_2)$ to q_2.

This performs quantum rotations on the qubits using the calculated angles, encoding the input numbers into the qubit states.

Step 5: Measure the system in the state $|10\rangle$. The coefficient should be calculated on the state vector, yielding half of the subtracted result, which can be doubled by applying a gain. However, the sign of the subtracted result is required for creating a comparator, and it is the same as the sign of its half. Consequently, doubling the result is unnecessary. This method involves measuring the quantum system to obtain a coefficient related to the difference.

2.6.3. The Quantum Sign Detector

The quantum sign detector is inspired by the Boolean subtraction operation, particularly focusing on the concept of the borrow, which is illustrated in the truth table. The borrow, denoted as r, is equal to 1 only when the minuend a is 0 and the subtrahend b is 1. The logical expression for the borrow can be represented as $r = \bar{a} \cdot b$. This expression indicates that a borrow occurs, meaning r equals 1, only if a is less than b. The quantum sign detector is inspired by the expression of the borrow of the Boolean subtraction, as described in the truth table depicted in Table 4.

Table 4. Truth table of the subtraction between two Boolean numbers.

a	b	$s = a - b$	r (Borrow)
0	0	0	0
0	1	1	1
1	0	1	0
1	1	0	0

In quantum computing, classical logic operations are translated into quantum gate operations. The purpose of the quantum sign detector is to implement the logic of the borrow operation using quantum gates, effectively detecting whether the result of a subtraction would require a borrow, which in classical terms, would indicate a negative result. Two key quantum gates are involved in this operation: the X gate (quantum NOT) and the CCNOT gate (Toffoli gate). The X gate is the quantum analogue of the classical NOT gate. It flips the state of a qubit; for instance, if the input qubit is in the $|0\rangle$ state, applying an X gate changes it to $|1\rangle$, and vice versa. In the context of the quantum sign detector, the X gate is used to invert the qubit representing a, producing $|\bar{a}\rangle$, which corresponds to the classical negation of a.

The CCNOT gate, or Toffoli gate, is a controlled-controlled-NOT gate. It performs a NOT operation on a target qubit only if the two control qubits are both in the $|1\rangle$ state. In the quantum sign detector, the CCNOT gate, takes $|\bar{a}\rangle$ and $|b\rangle$ as inputs and operates on an ancillary qubit initialized to $|0\rangle$. This operation effectively implements the logical AND between $\bar{a}$ and b, which corresponds to the classical borrow operation.

The quantum circuit for the sign detector operates as follows: Start by preparing qubits that represent the binary values a and b, along with an additional ancillary qubit initialized to $|0\rangle$. The qubit representing a is then passed through an X gate to obtain $|\bar{a}\rangle$. Subsequently, the CCNOT gate is applied to $|\bar{a}\rangle$ and $|b\rangle$, with the ancillary qubit as the target. The state of the ancillary qubit will be flipped to $|1\rangle$ if both $|\bar{a}\rangle = 1$ and $|b\rangle = 1$, thereby implementing the borrow logic. The final state of the ancillary qubit indicates the result of the quantum sign detection. If the ancillary qubit is in the $|1\rangle$ state, it corresponds to a borrow in the classical operation, signifying that the subtraction of b from a would result in a negative value. This quantum implementation of the borrow operation not only mirrors the classical logic but also leverages the principles of quantum

mechanics, such as parallelism and quantum efficiency. Figure 3 depicts the quantum sign detector in a quantum circuit.

Figure 3. The quantum sign detector circuit [56].

2.6.4. The Quantum Adder

To effectively implement the hysteresis function, a subtractor is required, which can be realized using an adder and a sign detector. The necessary components for the sign detection have already been developed in the context of the comparator function. Therefore, the remaining task is to develop the quantum adder. The addition of two real numbers, x and y, is achieved using trigonometric identities as illustrated in the following steps. This process is grounded in the principles of quantum mechanics, specifically leveraging the tensor product and quantum state measurements. The tensor product between quantum states q_1 and q_2 yields the coefficients of the eigenstates presented in Equation (38), and to focus on the addition process, we measure the system q_1q_2 in the state $|01\rangle$. This measurement can be reformulated using the following trigonometric identity:

$$S_{\theta_1}C_{\theta_2} = cos\left(\frac{\alpha-\beta}{2}\right)sin\left(\frac{\alpha+\beta}{2}\right) = \frac{1}{2}(sin(\alpha) + sin(\beta)) \quad (40)$$

Here, $\alpha = \theta_1 + \theta_2$ and $\beta = \theta_2 - \theta_1$. Therefore, the addition of two real numbers x and y, where $x = \sin(\alpha)$ and $y = \sin(\beta)$, is computed as follows:

Step 1: Compute $\alpha = \arcsin(x)$ and $\beta = \arcsin(y)$.

The real numbers x and y are first converted into angles α and β using the arcsine function, which is crucial for preparing the inputs for subsequent quantum operations.

Step 2: Calculate $\theta_1 = \frac{\alpha-\beta}{2}$ and $\theta_2 = \frac{\alpha+\beta}{2}$.

Using the computed angles α and β, the intermediary angles θ_1 and θ_2 are calculated and will define the quantum rotations applied to the qubits.

Step 3: Initialize quantum states q_1 and q_2 to 0.

The qubits q_1 and q_2 are initialized to the ground state $|0\rangle$. This initialization provides a known reference state for the quantum operations.

Step 4: Perform quantum rotations $R_y(\theta_1)$ on q_1 and $R_y(\theta_2)$ on q_2.

The rotations $R_y(\theta_1)$ and $R_y(\theta_2)$ are performed on the qubits q_1 and q_2, respectively. These rotations adjust the quantum states to encode the information about the original real numbers.

Step 5: Measure the system at the state $|01\rangle$. The measurement yields the coefficient of the state vector, representing half of the sum $x + y$. While the full addition result typically requires multiplying this coefficient by 2, in this context, only the sign of the result is necessary for constructing the hysteresis function. Hence, the multiplication by 2 can be omitted, as the sign of the result remains unchanged.

Developing a quantum adder is required for implementing advanced quantum functions. This process harnesses key quantum abilities such as superposition, interference, and measurement. The quantum adder can efficiently and simultaneously operate on multiple states, yielding precise and optimized outcomes that are often unachievable with

classical computing methods. The quantum system's capability to compute the sign of the sum without needing a full-scale addition underscores quantum computing's potential to simplify and enhance resource-intensive operations.

2.6.5. Proposed Quantum Algorithm

The quantum error e_Q is derived using a series of quantum operations that replace the classical error calculation. Let P denote the desired position and P_3 the actual position of the end-effector. The quantum error e_Q is calculated as follows:

For each axis i, compute the angles α_i and β_i corresponding to the components of P and P_3:

$$\alpha_i = arcsin\,(P_i) \tag{41}$$

$$\beta_i = arcsin(P_{3i}) \tag{42}$$

Next, calculate the rotation angles θ_{1i} and θ_{2i} as:

$$\theta_{1i} = \frac{\alpha_i - \beta_i}{2} \tag{43}$$

$$\theta_{2i} = \frac{\alpha_i + \beta_i}{2} \tag{44}$$

Two qubits q_{1i} and q_{2i} are initialized in the state $|0\rangle$ and the quantum rotations $Ry(\theta_{1i})$ and $Ry(\theta_{2i})$ are applied to these qubits, respectively:

$$q_{1i} = cos\,(\theta_{1i})|0\rangle + sin\,(\theta_{1i})|1\rangle \tag{45}$$

$$q_{2i} = cos\,(\theta_{2i})|0\rangle + sin\,(\theta_{2i})|1\rangle \tag{46}$$

The tensor product of these qubits is computed, and the system is measured in the state $|10\rangle$ to yield the quantum error component:

$$e_{Q_i} = k \cdot (q_{1i} \otimes q_{2i} \otimes q_{3i}) \tag{47}$$

Here the symbol $\otimes$ represents the tensor product, and k is a parametric term that can be adjusted to scale the quantum error component as needed for the specific requirements of the quantum control algorithm.

The derivative of the quantum error de_Q is computed using the quantum subtractor. Considering dP as the desired angular velocity and dP_Q as the quantum-calculated angular velocity obtained through the R_y gate, the derivative error de_Q is determined by the following relation:

$$de_Q = Quantum\ Subtractor\left(dP, dP_Q\right) \tag{48}$$

The quantum sliding surface $s_{quantum}$ is formed to approximate the classical sliding surface using quantum gates. First, the quantum error e_Q is scaled by a constant vector c:

$$scaled\ error = c \cdot e_Q \tag{49}$$

Then, the scaled quantum error and the quantum derivative error are added using quantum rotations. The resulting quantum sliding surface is expressed as:

$$s_{quantum} = n\left(sin\left(\frac{\theta_{c \cdot e}}{2}\right) + sin\left(\frac{\theta_{deQ}}{2}\right)\right) \tag{50}$$

Here, n is a parameter that can be tuned according to the specific requirements of the control system normalization, providing more flexibility in how the quantum sliding surface is scaled, and θ_{ce} and θ_{de} are the rotation angles for the scaled error and derivative error, respectively. The sign of the quantum sliding surface $s_{quantum}$ is detected using quantum computational techniques. The quantum state $|s\rangle$ representing the sliding surface is prepared as:

$$|s\rangle = cos\,(\theta)|0\rangle + sin\,(\theta)|1\rangle \tag{51}$$

where θ is calculated by the relation:

$$\theta = arcsin\left(\frac{s(t)}{max(|s(t)|)}\right) \tag{52}$$

The quantum sign detector then applies the X gate (quantum NOT gate) and the Toffoli gate (CCNOT gate) to determine the sign of the sliding surface. The outcome of the measurement after applying these gates indicates the sign of the sliding surface, with the ancillary qubit's state corresponding to +1 or −1.

The quantum control law u_Q is formulated by integrating the quantum sliding surface and the sign detection results. The control variable V is computed using the quantum sliding surface as:

$$V = J^{-1} \cdot \left(\ddot{P} + c \cdot de_Q + q \cdot Sign\left(s_Q\right) - \dot{J} \cdot \dot{q}\right) \tag{53}$$

where J is the Jacobian matrix, $\ddot{P}$ represents the desired acceleration, and $\dot{J} \cdot \dot{q}$ accounts for the effects of dynamic changes in the system.

The final control input u_Q is then calculated as:

$$u_Q = M \cdot V + B + G \tag{54}$$

So, M is the inertia matrix, B represents the Coriolis/centripetal forces, and G denotes the gravitational forces.

3. Results and Discussion

The following Simulink model is employed as the implementation algorithm for the carried-out simulation of the motion control of the robotic arm manipulator. Simulink allows creating blocks that have all the features and capabilities of any type of built-in function. The block function of the plant implemented all equations for the dynamic equations of motion, such as the inertia, gravity, and Coriolis centrifugal parameters, to obtain the torque and force equation of the robot presented in the kinematics and dynamic models of the robot in the methodology section of the current study and the mass properties of the robot, which consist of mass center points and inertia matrixes for the first three links presented in the section on CAO design and Table 3. A classic sliding-mode controller with the expositional reaching law approach based on the presented method is implemented in the controller block function, and the schematic diagram of the controller model is represented in Figure 4. Other Simulink models based on the quantum approach incorporating the quantum operators to handle the quantum version of the sliding-mode controller for the robot manipulator are designed and illustrated in Figure 5.

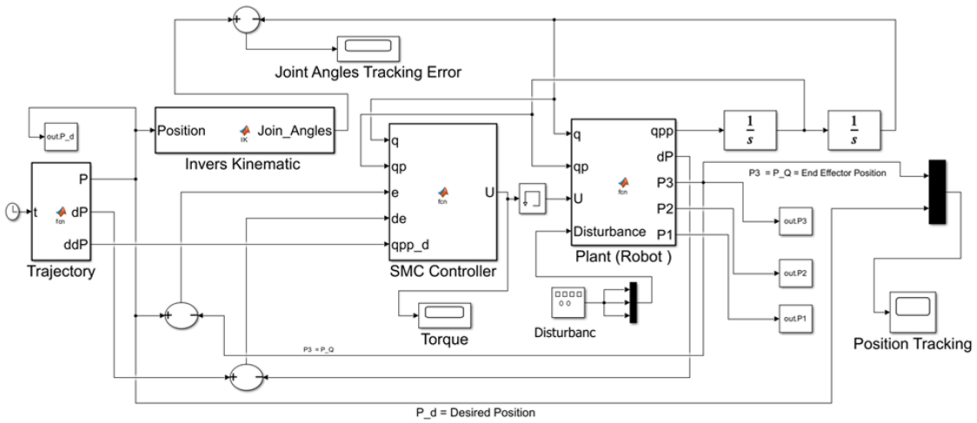

Figure 4. Simulink trajectory model of the robot manipulator for SMC.

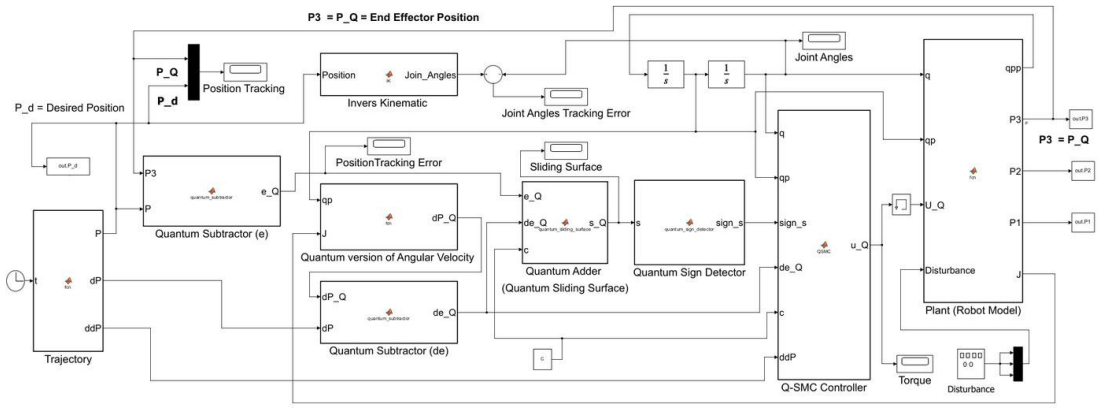

Figure 5. Simulink trajectory model of the robot manipulator for Q-SMC.

The sliding-mode controller algorithm is used for motion control based on a design with and without disturbances to evaluate the model's robustness. The value of disturbances applied based on the sine and cosine trajectory of the joint variable is predefined as a percentage of the input signal to examine the robustness of the designed controller. The implemented algorithm examines thoroughly a specific trajectory to verify the performance and behavior of the designed sliding-mode controllers of the robot to execute tasks undertaking the controllers. A circular trajectory is defined in the robot's working space considering avoiding singularity to perform the robot's task and estimate the chosen controller's execution. The motion of the end-effector begins at the same point for both controllers, positioned somewhere within the working space but outside the circular trajectory. Upon initiating the simulation, the robot attempts to reach the desired circular path, perform a circular motion along the defined trajectory, and maintain its position according to the specified parameters. The successful transition from an initial position outside the defined path to accurately following the specified circular trajectory within the robot's workspace confirms the correct operation of the controllers. Figure 6 illustrates the robot performing the assigned task under the SMC and Q-SMC controllers.

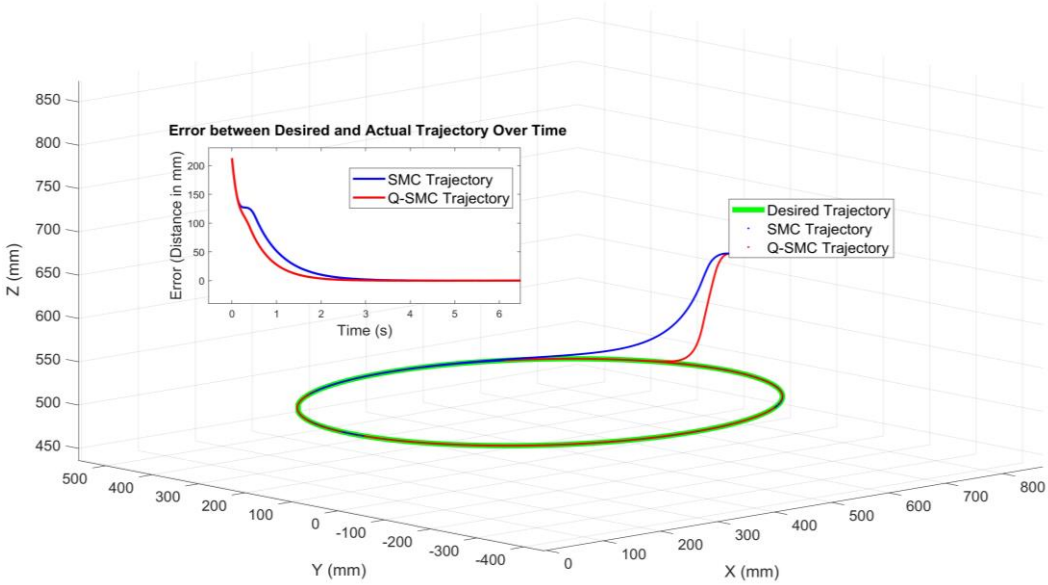

Figure 6. Projection of X–Y–Z trajectory of robot manipulator executed by controllers.

The Q-SMC aligns closely with the desired trajectory, guiding the robotic arm to precise coordinates, as the red dotted line shows. In contrast, the SMC controller, represented by the blue dotted line, exhibits delayed response and reduced accuracy, resulting in the arm deviating more noticeably from the intended path when reaching the coordinates.

Figures 7–9 illustrate the comparative position-tracking performance of the robotic arm's end-effector along the X, Y, and Z axes, employing both classic sliding-mode control and quantum-inspired sliding-mode control. The Q-SMC demonstrates superiority over the SMC in both transient and steady-state performance. As highlighted in the zoom-in inset, it achieves faster convergence to the desired trajectory with reduced overshoot. This enhancement is attributed to quantum-inspired innovations that facilitate smoother control actions and improved management of nonlinearities and disturbances.

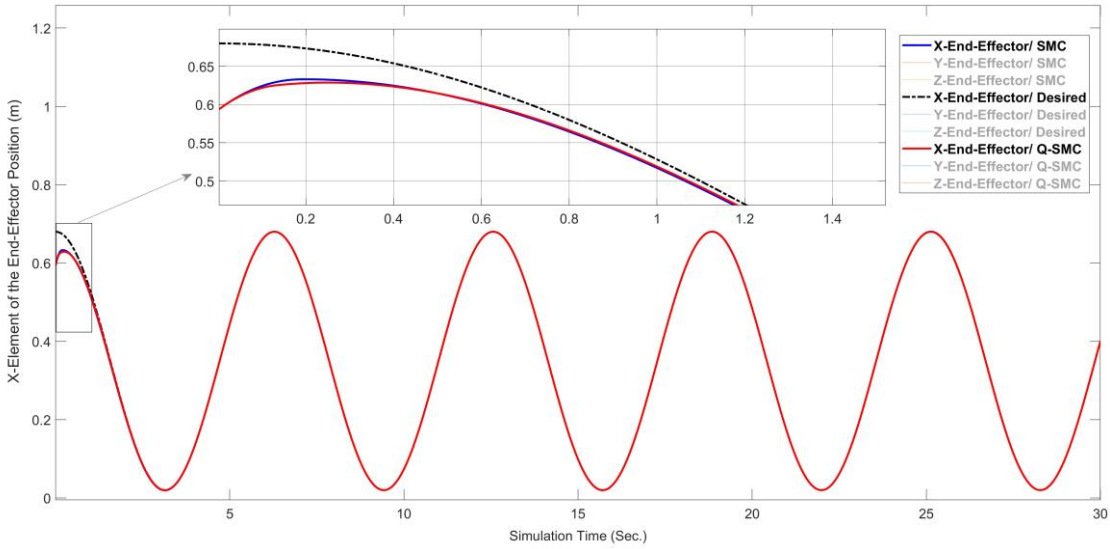

Figure 7. Comparison of position tracking (X–component) for the robot end-effector.

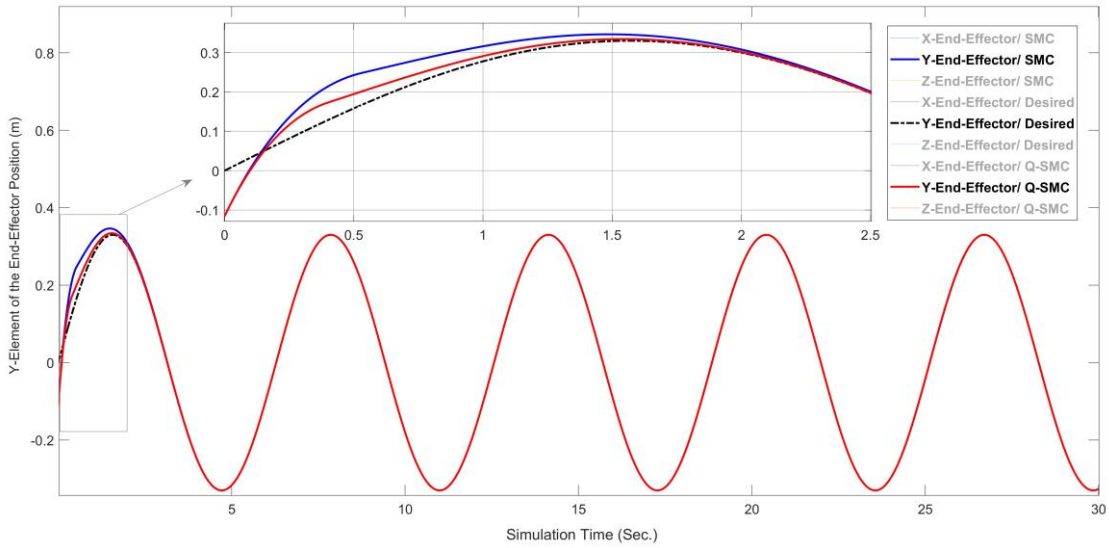

Figure 8. Comparison of position tracking (Y–component) for the robot end-effector.

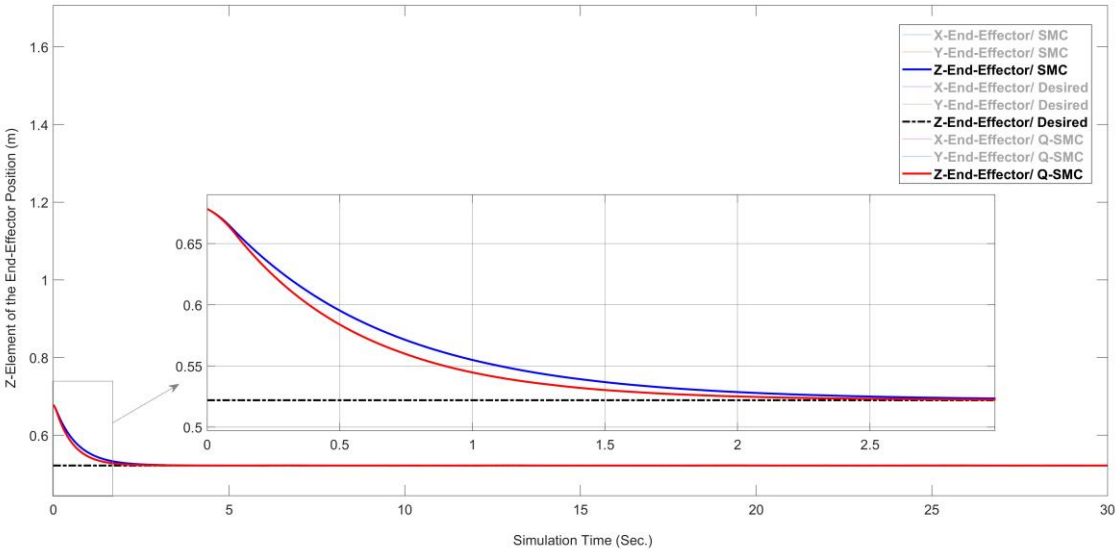

Figure 9. Comparison of position tracking (Z–component) for the robot end-effector.

Furthermore, Q-SMC maintains a closer adherence to the desired trajectory throughout the simulation, exhibiting exceptional tracking accuracy and robustness. The results along the *Y*-axis further underscore the benefits of Q-SMC, which delivers precise and smooth trajectory tracking. Consistently, Q-SMC outperforms SMC in terms of quicker convergence and reduced overshoot. The enhanced transient response and accurate path alignment are evident throughout the simulation. These improvements stem from the proposed controller's capacity to effectively mitigate uncertainties and disturbances, resulting in smoother and more dependable control actions.

In contrast, SMC displays slightly greater deviations from the desired trajectory, particularly during the transient phase, highlighting Q-SMC's superior precision and robustness. The quantum-inspired enhancements significantly reduce overshoot and oscillations, as depicted in the magnified transient response. Although both controllers ultimately achieve the target position, Q-SMC consistently provides better precision and stability throughout the simulation. The reduced chattering observed with Q-SMC decreases abrupt control actions, enhancing energy efficiency and preserving the mechanical integrity of the system. These findings reaffirm Q-SMC as a robust control strategy for applications requiring smooth and accurate trajectory tracking.

Figures 10–12 illustrate the tracking error of the robot's end-effector under both classical SMC and Q-SMC controllers. The results indicate that Q-SMC achieves a particularly lower steady-state error compared to SMC, showing improved tracking precision. While both controllers exhibit rapid error convergence, Q-SMC stabilizes more quickly with minimal oscillations, reflecting its enhanced robustness and smoother control actions. These findings underscore the effectiveness of the Q-SMC approach in maintaining trajectory accuracy, even in dynamic conditions.

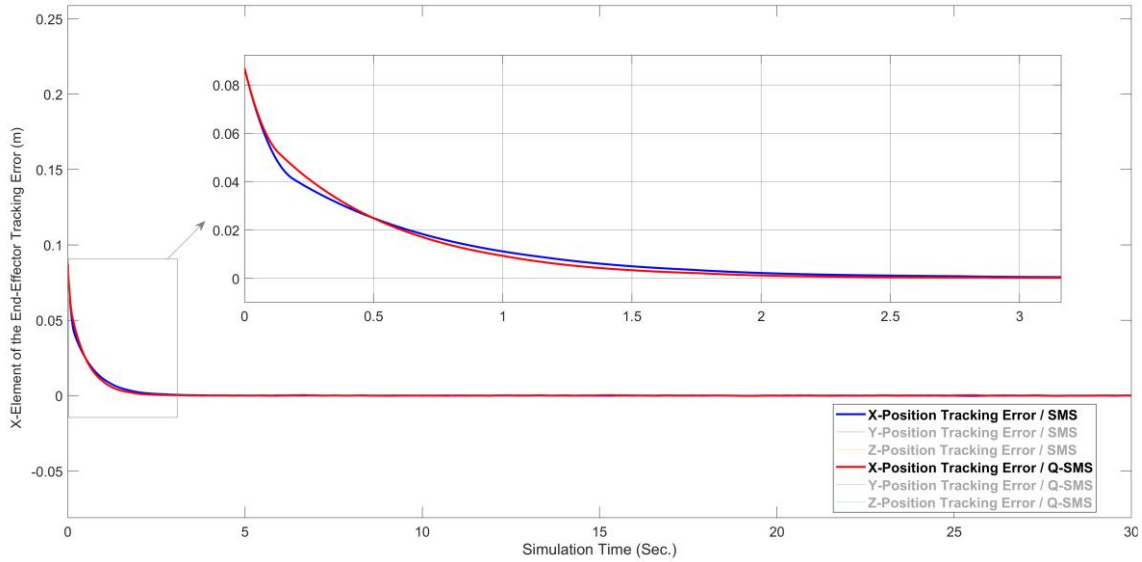

Figure 10. Comparison of tracking error (X–component) for the robot end-effector.

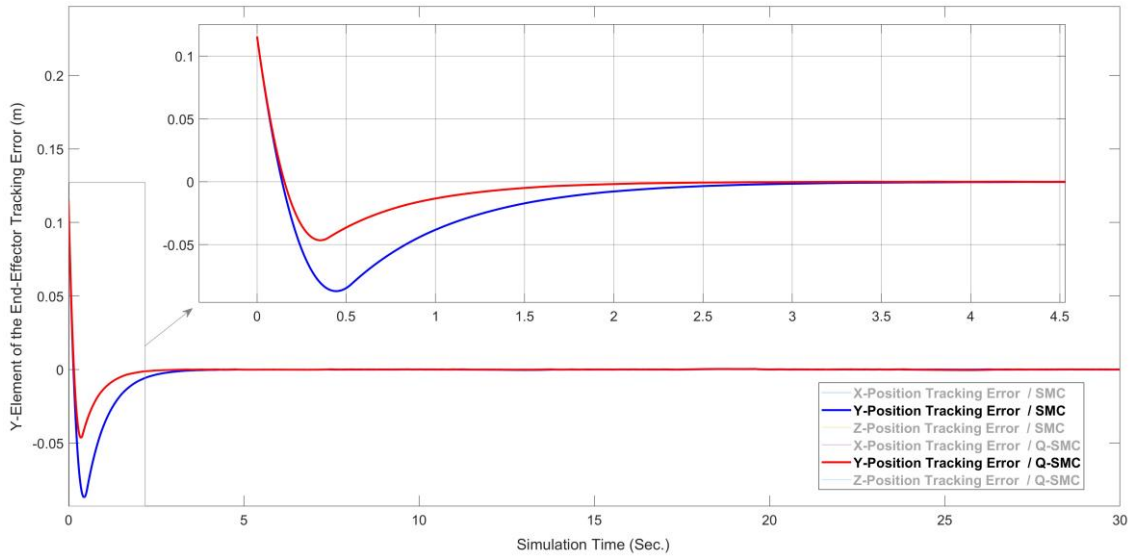

Figure 11. Comparison of tracking error (Y–component) for the robot end-effector.

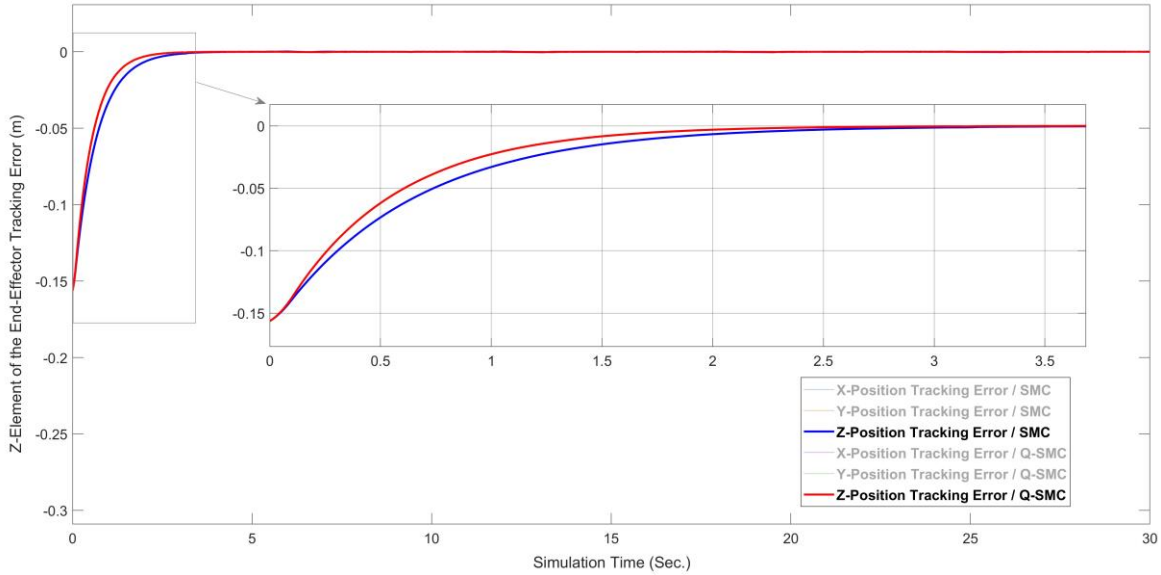

Figure 12. Comparison of tracking error (Z-component) for the robot end-effector.

Additionally, Q-SMC's reduced chattering and optimized control actions further validate it as a robust and precise control strategy for robotic systems. The classical SMC shows a notable initial overshoot in the Y-position, highlighting its greater sensitivity to sudden changes in system dynamics. In contrast, Q-SMC exhibits better stability, faster error convergence, and reduced fluctuations, resulting in a more consistent response over time. This difference in robustness allows Q-SMC to handle dynamic variations more efficiently and makes its smoother trajectory control particularly suitable for precision applications, solidifying its reputation as an advanced and effective control method for robotic systems.

The tracking performance for the Z-position of the robot's end-effector reveals that both controllers undergo a transient phase. However, Q-SMC achieves quicker convergence to near-zero errors and maintains a smoother trajectory. While classical SMC shows effectiveness, it experiences slight oscillations during stabilization, indicating a less refined response to system dynamics. In contrast, Q-SMC's ability to stabilize rapidly while managing smoother tracking errors underlines its precision and robustness, especially in addressing nonlinearities. These results further confirm the practicality of Q-SMC for applications that require high accuracy and reliability in robotic motion control.

Table 5 reviews the results of the classic and quantum sliding-mode controller performances. The comparison shows that the performances of both controllers are nearly identical. The evaluation of each controller's performance considers key metrics such as steady-state error, response speed, rise time, and settling time, addressing both time- and frequency-domain requirements. Considering all the measured parameters for both controllers when following the same trajectory, the Q-SMC model demonstrated superior performance.

Table 5. Performance of angular position for the different controllers.

Performances	Rising Time (s)	Settling Time (s)	Overshoot (%)	Steady-State Error (%)
		SMC		
Arm 1	0.301	0.42	1.76	0.088
Arm 2	0.297	0.79	2.09	0.076
Arm 3	0.302	0.53	1.97	0.066
		Q-SMC		
Arm 1	0.283	0.383	1.32	0.071

Arm 2	0.276	0.565	1.41	0.055
Arm 3	0.295	0.497	1.25	0.042

The controllers' ability to withstand modeling inaccuracies and unmodeled dynamics can be determined from their performance under disturbance conditions, albeit implicitly. In practical applications, the models used for controller design are usually approximations, making a controller's capability to maintain its performance despite such inaccuracies crucial. A control system's capacity to respond promptly and effectively to anticipated and unforeseen changes, including disturbances, is vital. This is particularly crucial in dynamic systems, where delays can result in significant errors or instability. The controllers' robustness is evaluated by analyzing their responses to disturbances, particularly when exposed to a sinusoidal disturbance set at 35% of the input signal. The performance response of the controllers under disturbance demonstrates satisfactory and appropriate behavior, as detailed in Table 6.

Table 6. Performance of angular position for the different controllers under disturbance.

Performances	Rising Time (s)	Settling Time (s)	Overshoot (%)	Steady-State Error (%)
		SMC		
Arm 1	0.525	0.579	1.85	0.0999
Arm 2	0.662	0.799	2.03	0.0807
Arm 3	0.515	0.598	1.97	0.0794
		Q-SMC		
Arm 1	0.454	0.691	1.39	0.0785
Arm 2	0.479	0.659	1.48	0.0551
Arm 3	0.463	0.623	1.28	0.0510

Upon reviewing the data in Tables 5 and 6, it is evident that the system's performance with and without disturbances is quite similar. However, in the presence of disturbances, the steady-state error increased to 10.71% for the quantum sliding-mode controller and 12.13% for the classical sliding-mode controller. The overshoot remained unchanged, while the rise times increased by an average of 0.2 s. Similarly, in the scenario without disturbances, the controllers displayed comparable response and reaching times under disturbance conditions for the same trajectory execution and initial conditions.

Both controllers display worthy robustness in the presence of disturbances, maintaining low tracking errors even under substantial disturbances. The analysis of the response plots highlights several required characteristics relevant to the design and assessment of control systems. Notably, the transient response analysis indicates that Q-SMC outperforms SMC by achieving a faster settling time with fewer instabilities, suggesting that the improved damping characteristics of Q-SMC enable it to bring the system to a steady state more efficiently. Additionally, Q-SMC consistently minimizes steady-state error, ensuring greater accuracy in tracking the desired trajectory. This feature is advantageous in precision engineering applications, where performance and implementation complexity are key in real-world implementations such as robotics; the selection or design of controllers must consider these factors. Moreover, despite being often overlooked, energy efficiency is vital, especially in systems that operate continuously or under power constraints. The smoother control action and reduced oscillations observed in Q-SMC suggest it is more energy-efficient than conventional SMC.

Figures 13–16 represent the torque control signals for individual robotic arm joints and the robot's total torque, providing essential insights into the performance and efficiency of the evaluated control strategies under 35% of input signal disturbances.

Outcomes show how the controllers, SMC and Q-SMC, manage the dynamic requirements of individual joints under defined trajectories, recalling the smoothness, oscillations, and magnitude of the torque values that indicate the control algorithms' efficiency in handling nonlinearities and disturbances. The total torque across all joints offers a close view of the robotic arm's overall dynamic load and energy exertion, which is crucial for comparing the total effort required by SMC versus Q-SMC to achieve the same task and conditions. These figures are important for performance evaluation, as the torque signals indicate the system's ability to handle nonlinear dynamics, ensure smooth control actions, and resist chattering issues typically associated with classical SMC. The data can further enable energy efficiency analysis by linking torque values directly to the robot's energy consumption, showcasing how well the control system manages resources. Additionally, the formations accentuate the robustness of Q-SMC under disturbance scenarios, highlighting its capability to preserve stable arrangements without significant oscillations or overshoot.

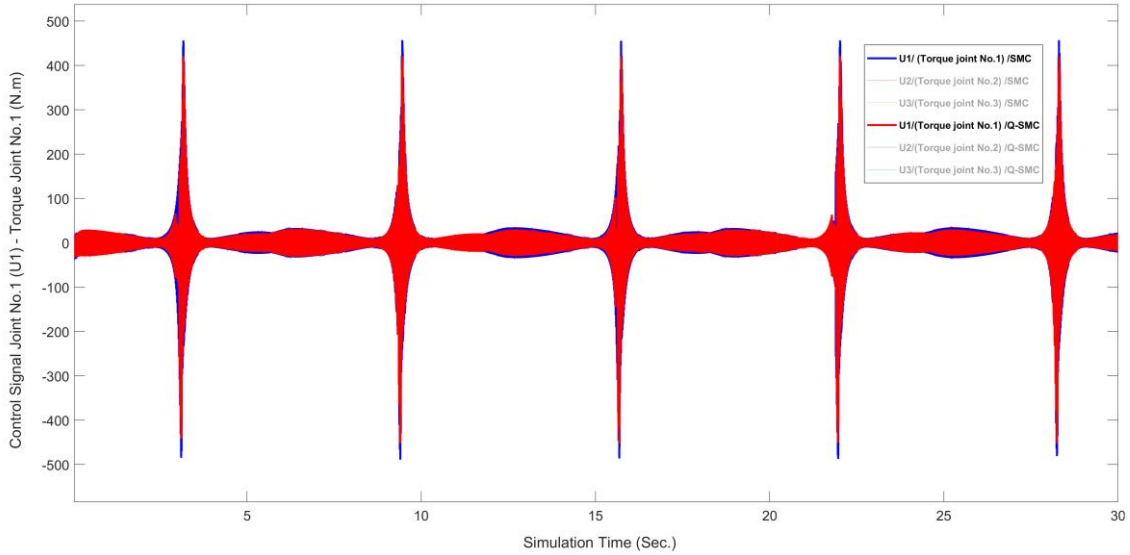

Figure 13. Control signals for joint 1 for SMC and Q-SMC controllers under disturbance.

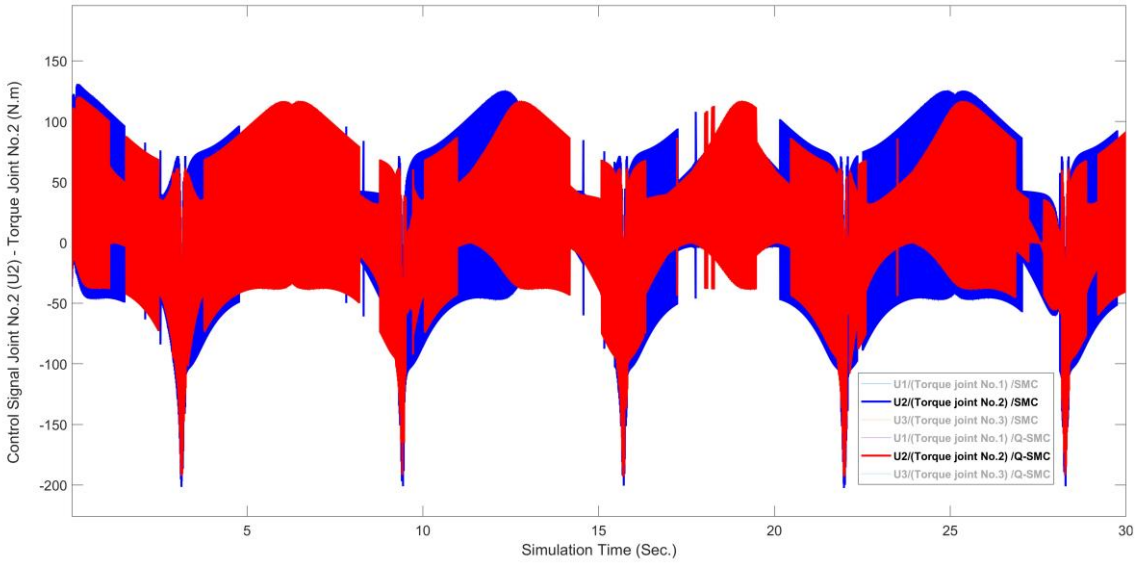

Figure 14. Control signals for joint 2 for SMC and Q-SMC controllers under disturbance.

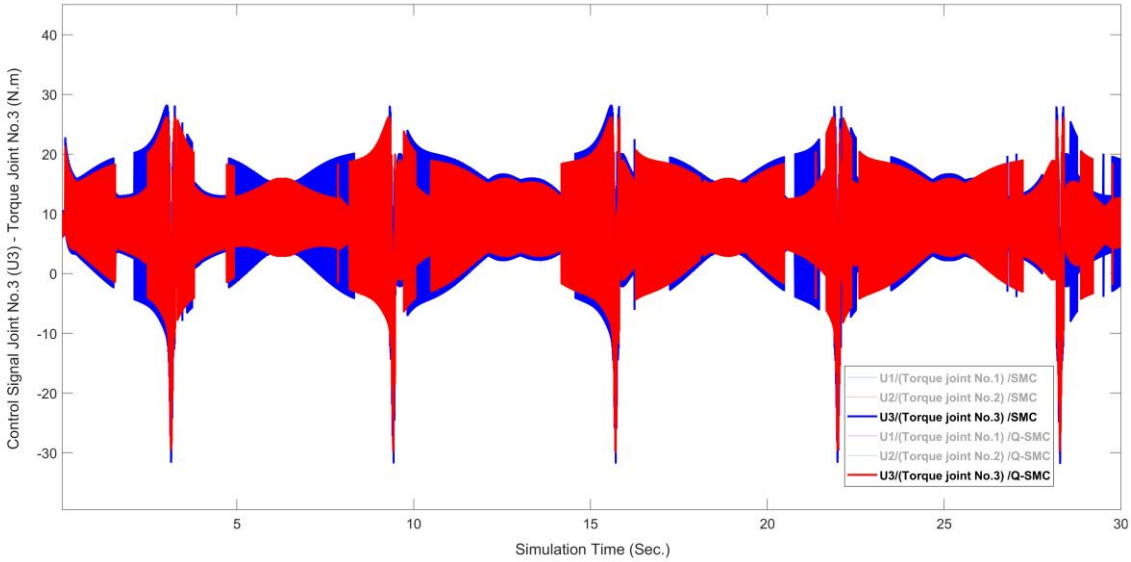

Figure 15. Control signals for joint 3 for SMC and Q-SMC controllers under disturbance.

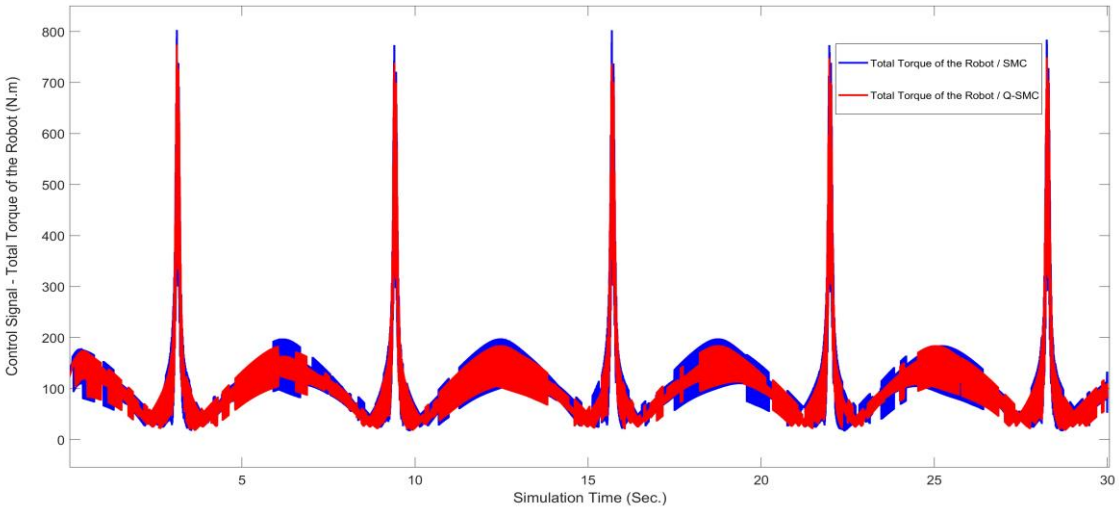

Figure 16. Control signals for the robot under SMC and Q-SMC controllers under disturbance.

These advancements improve the precision and stability of the robotic manipulator while minimizing mechanical wear and stress, ultimately extending the operational lifespan of the robotic components. As a result, both approaches are particularly well-suited for enhancing trajectory tracking precision in high-precision industrial applications and complex robotic systems. The findings emphasize the superior robustness and adaptability of Q-SMC, showcasing its potential to excel in high-performance dynamic environments.

In terms of total torque profiles, the Q-SMC consistently outperforms classical SMC by generating more stable and efficient control signals that effectively reject disturbances while maintaining system stability. Collectively, these results demonstrate Q-SMC's enhanced performance in overcoming the limitations of classical SMC, offering improved stability, precision, and efficiency. Its ability to effectively surpass chattering positions Q-SMC as a promising advancement for robust control in industrial automation and other high-performance sectors in dynamic and disturbance-prone environments.

Estimating the energy consumption of robotic systems across various controllers is essential for assessing the efficiency and effectiveness of these control strategies. By analyzing the total energy drawn from the robot's torque profile needed to perform identical

trajectories, we can gain valuable insights into the effectiveness of each controller in managing the complex dynamics of robotic systems. Energy consumption is directly related to the operational demands placed on the controller, including the forces and torques required for precise movements, especially when faced with disturbances. A control strategy that minimizes energy usage while preserving or enhancing system performance indicates superior efficiency, contributing to the robot's performance and reliability. This approach provides a comprehensive framework for considering the balance between control precision, robustness, and energy efficiency, establishing a clear benchmark for optimizing robotic implementation.

Figure 17 shows the total energy consumption of the robotic system under disturbance conditions operated by both the SMC and Q-SMC based on the robot performance assessment presented in relation (2). The illustration proves that the Q-SMC provides a more stable energy profile and decreases total energy consumption compared to the classical SMC. Particularly, the robot under the Q-SMC controller consumed approximately 3.79% less energy than the classical SMC controller. This reduction is noteworthy as it underlines the quantum approach's capability to enhance energy efficiency while maintaining or even enhancing control accuracy. These findings indicate that the Q-SMC effectively reduced the effects of disturbances and optimized energy usage, leading to a more sustainable and reliable control strategy. This advancement in energy management is required for the long-term operation of robotic systems, as it suggests reduced wear on mechanical components and a more environmentally tolerable approach to robotic control. The results highlight the potential of quantum-inspired control methods in advancing the field of robotics, particularly in applications where energy efficiency is as essential as precision and robustness.

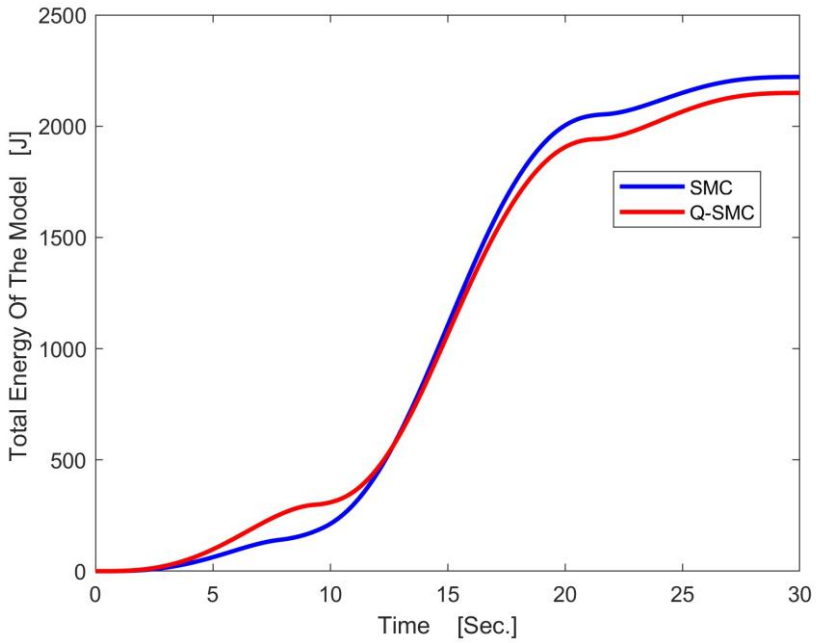

Figure 17. Total energy of the robot run by controllers under disturbance.

Q-SMC has demonstrated superior energy efficiency compared to SMC. This is particularly advantageous for battery-powered robots, allowing longer operational durations without recharging. Furthermore, reducing energy consumption leads to cost savings and a decrease in heat generation in industrial environments, ultimately extending the lifespan of robotic components. This enhanced energy efficiency also promotes environmental sustainability by reducing the dependence on non-renewable energy sources. It

plays a significant role in ensuring the overall reliability and longevity of robotic systems, especially in high-precision applications where maintaining mechanical integrity is critical.

In a comprehensive and overarching manner, the principle of superposition facilitates the simultaneous representation of multiple potential system states, thereby increasing the control algorithm's capacity to respond to dynamic changes. Within the Q-SMC framework, superposition is utilized to encode the robotic end-effector's desired and actual states into a unified quantum state. The quantum error computation detailed in Equations (41)–(47) exemplifies this principle, as it allows for concurrent analysis of multiple input trajectories, enabling rapid and precise error evaluation. This comprehensive error assessment mechanism enhances trajectory tracking, promoting faster convergence to the desired path and mitigating transient overshoot. As evidenced in Figures 7–12 and Tables 5 and 6, Q-SMC outperforms classical SMC, demonstrating superior tracking precision and smoother control transitions, affirming superposition's efficacy in optimizing control dynamics with or without disturbances.

Entanglement establishes a foundational relation between interdependent control variables, such as error signals and their derivatives, ensuring seamless synchronization for dynamic responsiveness. In the Q-SMC framework, this principle is operationalized through the quantum comparator and sign detector presented in Sections 2.6.1–2.6.3, enabling the real-time alignment of quantum error and its derivative. This synchronization ensures that adjustments to the sliding surface accurately mirror dynamic changes in the robotic system, resulting in minimizing control response delays. Accordingly, Q-SMC consistently delivers precise and stable control actions characterized by reduced trajectory deviations and improved steady-state accuracy. The benefits of entanglement's influence are shown in Figures 9–12, where the Q-SMC exhibits robust stability during transient phases, effectively accommodating dynamic variations and reinforcing its advanced adaptability for complex control scenarios.

The computational efficiency of Q-SMC derives from the strategic utilization of quantum gates, including Hadamard and rotation gates, which enable intricate mathematical operations such as error scaling and derivative computation. These gates manipulate the intrinsic parallelism of quantum mechanics, allowing the controller to process high-dimensional data in real-time with minimal computational load. For instance, the quantum subtractor in Equations (36)–(39) adeptly computes trajectory differences, generating precise and responsive control signals. This computational optimization translates directly into the observed smoother control transitions and significantly reduced delays, as illustrated in Figures 13–16, emphasizing the practical benefits of integrating quantum gates into the control framework.

Chattering, a general challenge in classical SMC, is effectively reduced in Q-SMC by involving the exponential reaching law combined with a saturation function. This methodology establishes a boundary layer around the sliding surface and smoothens the transitions in control inputs, thereby minimizing the abrupt variations that cause chattering. This refinement, drawing stimulation from quantum error correction, enhances the system's energy efficiency and preserves the robotic components' mechanical integrity. As depicted in Figures 13–16, the torque profiles produced by Q-SMC exhibit considerably smoother characteristics compared to those generated by classical SMC. Additionally, the system's enhanced energy efficiency is quantified in Figure 17, where Q-SMC displays a 3.79% reduction in total energy consumption, emphasizing its superior performance in energy-sensitive and precision-demanding applications.

4. Conclusions

The present study aimed to evaluate the effectiveness of quantum-inspired sliding-mode control in enhancing the robustness, accuracy, and computational efficiency of control methods for articulated robotic arms, focusing specifically on a six-degree-of-freedom robotic manipulator. By integrating quantum principles into the conventional sliding-mode control framework, the research addressed persistent issues such as chattering, computational complexity, and robustness against disturbances. The methodology involved the development of a comprehensive kinematic and dynamic model of the robotic arm, followed by the implementation and comparison of both classic SMC and Q-SMC through extensive simulations. The findings provide valuable insights into the potential of quantum-inspired approaches in advancing robotic control systems.

The results revealed several significant findings. Most notably, Q-SMC outperformed the classic SMC in key areas such as precision, robustness, and energy efficiency. Q-SMC effectively mitigated the chattering phenomenon, a common issue in classic SMC, resulting in smoother and more precise control of the robotic arm. Additionally, Q-SMC confirmed quicker response times and lower steady-state errors, showcasing its improved capability to handle the nonlinear dynamics and external disturbances inherent in robotic systems. The torque profile and energy consumption analysis further highlighted the efficiency of Q-SMC, with the robotic arm consuming approximately 3.79% less energy under Q-SMC compared to classic SMC.

These findings have important implications for both theoretical and practical applications in the field of robotics and control systems. Theoretically, this study contributes to the existing body of knowledge by introducing a novel application of quantum principles to sliding-mode control, advancing our understanding of how quantum computing techniques can enhance control system performance. This opens new avenues for the design and optimization of robust controllers. Practically, implementing Q-SMC could lead to technological advancements in robotic systems, particularly in applications requiring high precision and reliability, such as industrial automation, medical robotics, and aerospace. Furthermore, the reduced energy consumption associated with Q-SMC suggests potential benefits for developing more sustainable and efficient robotic systems.

However, it is important to acknowledge certain limitations of the study, primarily due to its execution in a simulated environment. While the models employed were comprehensive, they may not fully capture the complexities of real-world scenarios. Additionally, the application of quantum-inspired algorithms was constrained by current computational capabilities, which may limit the generalizability of the findings to other types of robotic systems or more complex environments. These limitations suggest that further validation through experimental setups is necessary to confirm the effectiveness and relevance of Q-SMC in real-world applications.

Recognizing the crucial importance of experimental validation, we are committed to bridging the gap between simulations and real-world applications. According to the promising simulation results presented in this study, our future work will focus on incorporating other advanced strategies; we prioritized depth over breadth in this initial study, validating Q-SMC for high-precision tasks such as trajectory tracking and energy-efficient path execution under varying loads and disturbances. To ensure comparability, we will replicate simulation conditions and evaluate real-world performance using a hybrid classical–quantum framework, where computationally intensive components are executed on available quantum platforms. Performance metrics include chattering reduction, trajectory tracking accuracy, and energy efficiency. Beyond the specific case study examined here, we aim to expand Q-SMC's applicability to diverse robotic platforms and tasks, including industrial applications like assembly and welding, to explore scalability and versatility.

In conclusion, the findings underscore the robust control capabilities of both conventional sliding-mode control and quantum-inspired sliding-mode control for robotic arms. While SMC is well known for its robustness, the proposed Q-SMC demonstrates superior accuracy, precision, and an enhanced ability to address common challenges like chattering. Q-SMC significantly improves the stability and precision of the control system, particularly in dynamic, disturbance-prone environments. Its smoother control actions contribute to the overall better performance of the robotic arm, resulting in faster response times, reduced steady-state errors, and lower energy consumption, making it a more practical and effective technique for achieving high-performance robotic control.

Author Contributions: M.F. contributed to conceptualization, methodology, investigation, formal analysis, writing and editing of the original draft, and visualization. N.Z. contributed to providing resources, supervision, project administration, formal analysis, review and editing of the original draft, funding acquisition, and visualization. All authors have read and agreed to the published version of the manuscript.

Funding: This work was financially supported by NSERC Canada.

Data Availability Statement: The data supporting the findings of this study are not publicly available as they are part of ongoing research and future work. Data may be shared upon reasonable request after the completion of future studies.

Conflicts of Interest: The authors declare no conflicts of interest.

Abbreviations

The following abbreviations are used in this manuscript:

SMC	Sliding-Mode Control
QSMC	Quantum Sliding-Mode Control
CAD	Computer-Aided Design
CAO	Computer-Aided Optimization
CAM	Computer-Aided Manufacturing
CCNOT	Controlled-Controlled-Not
DH	Denavit–Hartenberg

References

1. Anh, H.P.H.; Van Kien, C.; Son, N.N.; Nam, N.T. New approach of sliding mode control for nonlinear uncertain pneumatic artificial muscle manipulator enhanced with adaptive fuzzy estimator. *Int. J. Adv. Robot. Syst.* **2018**, *15*, 1729881418773204.
2. Azeez, M.I.; Abdelhaleem, A.M.M.; Elnaggar, S.; Moustafa, K.A.F.; Atia, K.R. Optimized sliding mode controller for trajectory tracking of flexible joints three-link manipulator with noise in input and output. *Sci. Rep.* **2023**, *13*, 12518.
3. Ajwad, S.A.; Iqbal, J.; Islam, R.U.; Alsheikhy, A.; Almeshal, A.; Mehmood, A. Optimal and robust control of multi DOF robotic manipulator: Design and hardware realization. *Cybern. Syst.* **2018**, *49*, 77–93.
4. Liu, Z.; Peng, K.; Han, L.; Guan, S. Modeling and control of robotic manipulators based on artificial neural networks: A review. *Iran. J. Sci. Technol. Trans. Mech. Eng.* **2023**, *47*, 1307–1347.
5. Wang, X.; Wang, D.; Du, M.; Song, K.; Ni, Y.; Li, Y. A two-layer trajectory tracking control scheme of manipulator based on elm-smc for autonomous robotic vehicle. *IEEE Trans. Autom. Sci. Eng.* **2023**, *21*, 2337–2348.
6. Ravandi, A.K.; Khanmirza, E.; Daneshjou, K. Hybrid force/position control of robotic arms manipulating in uncertain environments based on adaptive fuzzy sliding mode control. *Appl. Soft Comput.* **2018**, *70*, 864–874.
7. Kumar, R.; Kumar, K. Design and control of a two-link robotic manipulator: A review. *AIP Conf. Proc.* **2021**, *2358*, 050020.
8. Abdelmaksoud, S.I.; Al-Mola, M.H.; Abro, G.E.M.; Asirvadam, V.S. In-Depth Review of Advanced Control Strategies and Cutting-Edge Trends in Robot Manipulators: Analyzing the Latest Developments and Techniques. *IEEE Access* **2024**, *12*, 47672–47701.
9. Abbas, N.; Abbas, Z.; Zafar, S.; Ahmad, N.; Liu, X.; Khan, S.S.; Foster, E.D.; Larkin, S. Survey of Advanced Nonlinear Control Strategies for UAVs: Integration of Sensors and Hybrid Techniques. *Sensors* **2024**, *24*, 3286.

10. Zaihidee, F.M.; Mekhilef, S.; Mubin, M. Robust speed control of PMSM using sliding mode control (SMC)—A review. *Energies* **2019**, *12*, 1669.
11. Fazilat, M.; Zioui, N. The Impact of Simplifications of the Dynamic Model on the Motion of a Six-Jointed Industrial Articulated Robotic Arm Movement. *J. Robot. Control (JRC)* **2024**, *5*, 173–186.
12. Vijay, M.; Jena, D. Backstepping terminal sliding mode control of robot manipulator using radial basis functional neural networks. *Comput. Electr. Eng.* **2018**, *67*, 690–707.
13. Adhikary, N.; Mahanta, C. Sliding mode control of position commanded robot manipulators. *Control Eng. Pract.* **2018**, *81*, 183–198.
14. Norsahperi, N.; Danapalasingam, K. An improved optimal integral sliding mode control for uncertain robotic manipulators with reduced tracking error, chattering, and energy consumption. *Mech. Syst. Signal Process.* **2020**, *142*, 106747.
15. Truong, T.N.; Vo, A.T.; Kang, H.-J. A backstepping global fast terminal sliding mode control for trajectory tracking control of industrial robotic manipulators. *IEEE Access* **2021**, *9*, 31921–31931.
16. Baek, J.; Kwon, W.; Kang, C. A new widely and stably adaptive sliding-mode control with nonsingular terminal sliding variable for robot manipulators. *IEEE Access* **2020**, *8*, 43443–43454.
17. Baek, J.; Kwon, W. Practical adaptive sliding-mode control approach for precise tracking of robot manipulators. *Appl. Sci.* **2020**, *10*, 2909.
18. Feng, Y.; Zhou, M.; Yu, X.; Han, F. Full-order sliding-mode control of rigid robotic manipulators. *Asian J. Control* **2019**, *21*, 1228–1236.
19. Zhai, J.; Li, Z. Fast-exponential sliding mode control of robotic manipulator with super-twisting method. *IEEE Trans. Circuits Syst. II Express Briefs* **2021**, *69*, 489–493.
20. Soriano, L.A.; Rubio, J.d.J.; Orozco, E.; Cordova, D.A.; Ochoa, G.; Balcazar, R.; Cruz, D.R.; Meda-Campaña, J.A.; Zacarias, A.; Gutierrez, G.J. Optimization of sliding mode control to save energy in a SCARA robot. *Mathematics* **2021**, *9*, 3160.
21. Yen, V.T.; Nan, W.Y.; Van Cuong, P. Recurrent fuzzy wavelet neural networks based on robust adaptive sliding mode control for industrial robot manipulators. *Neural Comput. Appl.* **2019**, *31*, 6945–6958.
22. Jung, S. Improvement of tracking control of a sliding mode controller for robot manipulators by a neural network. *Int. J. Control Autom. Syst.* **2018**, *16*, 937–943.
23. Gambhire, S.J.; Kishore, D.R.; Londhe, P.S.; Pawar, S.N. Review of sliding mode based control techniques for control system applications. *Int. J. Dyn. Control* **2021**, *9*, 363–378.
24. Yu, X.; Feng, Y.; Man, Z. Terminal sliding mode control—An overview. *IEEE Open J. Ind. Electron. Soc.* **2020**, *2*, 36–52.
25. Yin, F.; Wen, C.; Ji, Q.; Zhang, H.; Shao, H. A compensation sliding mode control for machining robotic manipulators based on nonlinear disturbance observer. *Trans. Inst. Meas. Control* **2022**, *44*, 2336–2349.
26. Gan, W.; Zhu, D.; Ji, D. QPSO-model predictive control-based approach to dynamic trajectory tracking control for unmanned underwater vehicles. *Ocean Eng.* **2018**, *158*, 208–220.
27. Fazilat, M.; Zioui, N.; St-Arnaud, J. A novel quantum model of forward kinematics based on quaternion/Pauli gate equivalence: Application to a six-jointed industrial robotic arm. *Results Eng.* **2022**, *14*, 100402.
28. Zioui, N.; Mahmoudi, A.; Tadjine, M. Representing quantum spins in different coordinate systems for modelling rigid body orientation. *Karbala Int. J. Mod. Sci.* **2023**, *9*, 11.
29. Boudjoghra, M.E.A.; Daimellah, S.A.S.; Zioui, N.; Mahmoudi, Y.; Tadjine, M. State-Domain Equations and Their Quantum Computing Solution Based HHL Algorithm. *Math. Model. Eng. Probl.* **2022**, *9*, 879–886.
30. Singh, R.; Sloth, C. Characterizing Manipulator Motion Using an Evolving Type 2 Quantum Fuzzy Neural Network. In Proceedings of the 2024 IEEE/SICE International Symposium on System Integration (SII), Ha Long, Vietnam, 8–11 January 2024.
31. Zheng, X.; Su, X. Sliding mode control of electro-hydraulic servo system based on optimization of quantum particle swarm algorithm. *Machines* **2021**, *9*, 283.
32. Qu, Q.; Chen, F.; Jiang, B.; Tao, G. Integral sliding mode control for helicopter via disturbance observer and quantum information technique. *Math. Probl. Eng.* **2015**, *2015*, 938246.
33. Zioui, N.; Mahmoudi, Y.; Mahmoudi, A.; Tadjine, M.; Bentouba, S. A novel quantum-computing-based quaternions model for a robotic arm position. *Int. J. Comput. Intell. Control* **2021**, *13*, 71–77.
34. Sivak, V.V.; Eickbusch, A.; Liu, H.; Royer, B.; Tsioutsios, I.; Devoret, M.H. Model-free quantum control with reinforcement learning. *Phys. Rev. X* **2022**, *12*, 011059.

35. Petschnigg, C.; Brandstötter, M.; Pichler, H.; Hofbaur, M.; Dieber, B. Quantum computation in robotic science and applications. In Proceedings of the 2019 International Conference on Robotics and Automation (ICRA), Montreal, QC, Canada, 20–24 May 2019.
36. Niu, M.Y.; Boixo, S.; Smelyanskiy, V.N.; Neven, H. Universal quantum control through deep reinforcement learning. *Npj Quantum Inf.* **2019**, *5*, 33.
37. Reshetnikov, A.; Ulyanov, S. Quantum Algorithm of Imperfect KB Self-organization. Pt II: Robotic Control with Remote Knowledge Base Exchange. *Artif. Intell. Adv.* **2021**, *3*, 44–70.
38. Tavanaei-Sereshki, Z.; Ramezani-Al, M.R. Quantum genetic sliding mode controller design for depth control of an underwater vehicle. *Meas. Control.* **2018**, *51*, 336–348.
39. Xi, R.-D.; Xiao, X.; Ma, T.-N.; Yang, Z.-X. Adaptive sliding mode disturbance observer based robust control for robot manipulators towards assembly assistance. *IEEE Robot. Autom. Lett.* **2022**, *7*, 6139–6146.
40. Haviland, J.; Corke, P. Manipulator Differential Kinematics: Part I: Kinematics, Velocity, and Applications. *IEEE Robot. Autom. Mag.* **2023**, *31*, 149–158.
41. Zaare, S.; Soltanpour, M.R.; Moattari, M. Adaptive sliding mode control of n flexible-joint robot manipulators in the presence of structured and unstructured uncertainties. *Multibody Syst. Dyn.* **2019**, *47*, 397–434.
42. Ranjbar, E.; Suratgar, A.A.; Menhaj, M.B.; Prasad, M. Design of a fuzzy adaptive sliding mode control system for MEMS tunable capacitors in voltage reference applications. *IEEE Trans. Fuzzy Syst.* **2021**, *30*, 1838–1852.
43. Wu, L.; Liu, J.; Vazquez, S.; Mazumder, S.K. Sliding mode control in power converters and drives: A review. *IEEE/CAA J. Autom. Sin.* **2021**, *9*, 392–406.
44. Zhao, Y.; Wang, J.; Cao, G.; Yuan, Y.; Yao, X.; Qi, L. Intelligent control of multilegged robot smooth motion: A review. *IEEE Access* **2023**, *11*, 86645–86685.
45. Costa-Castello, R.; Carrero, N.; Dormido, S.; Fossas, E. Teaching, analyzing, designing and interactively simulating sliding mode control. *IEEE Access* **2018**, *6*, 16783–16794.
46. Marques, F.; Flores, P.; Claro, J.C.P.; Lankarani, H.M. A survey and comparison of several friction force models for dynamic analysis of multibody mechanical systems. *Nonlinear Dyn.* **2016**, *86*, 1407–1443.
47. Truong, T.N.; Vo, A.T.; Kang, H.-J. Neural network-based sliding mode controllers applied to robot manipulators: A review. *Neurocomputing* **2023**, *562*, 126896.
48. Sciavicco, L.; Siciliano, B. *Modelling and Control of Robot Manipulators*; Springer Science & Business Media: Berlin/Heidelberg, Germany, 2012.
49. Feraoun, H.; Fazilat, M.; Dermouche, R.; Bentouba, S.; Tadjine, M.; Zioui, N. Quantum maximum power point tracking (QMPPT) for optimal solar energy extraction. *Syst. Soft Comput.* **2024**, *6*, 200118.
50. Reda, D.; Talaoubrid, A.; Fazilat, M.; Zioui, N.; Tadjine, M. A quantum direct torque control method for permanent magnet synchronous machines. *Comput. Electr. Eng.* **2025**, *122*, 109994.
51. Ahmadpour, S.-S.; Noorallahzadeh, M.; Al-Khafaji, H.M.R.; Darbandi, M.; Navimipour, N.J.; Javadi, B.; Ain, N.U.; Hosseinzadeh, M.; Yalcin, S. A new energy-efficient design for quantum-based multiplier for nano-scale devices in internet of things. *Comput. Electr. Eng.* **2024**, *117*, 109263.
52. Ahmadpour, S.-S.; Navimipour, N.J. A new nano-design of 16-bit carry look-ahead adder based on quantum technology. *Phys. Scr.* **2023**, *98*, 125108.
53. Orts, F.; Ortega, G.; Cucura, A.C.; Filatovas, E.; Garzón, E.M. Optimal fault-tolerant quantum comparators for image binarization. *J. Supercomput.* **2021**, *77*, 8433–8444.
54. Yuan, Y.; Wang, C.; Wang, B.; Chen, Z.-Y.; Dou, M.-H.; Wu, Y.-C.; Guo, G.-P. An improved QFT-based quantum comparator and extended modular arithmetic using one ancilla qubit. *New J. Phys.* **2023**, *25*, 103011.
55. Ahmadpour, S.-S.; Navimipour, N.J.; Kerestecioglu, F. A new nano-design of an efficient synchronous full-adder/subtractor based on quantum-dots. *Eurasia Proc. Sci. Technol. Eng. Math.* **2023**, *22*, 81–86.
56. IBM Quantum Composer. 2024. Available online: https://quantum.ibm.com/composer/files/new (Accessed on 26 January 2025.)